Experimental Thermal and Fluid Science 74 (2016) 27–48

Contents lists available at ScienceDirect

Experimental Thermal and Fluid Science

journal homepage: www.elsevier.com/locate/etfs

Bubble size distributions and shapes in annular gap bubble column

Giorgio Besagni *, Fabio Inzoli

Politecnico di Milano, Department of Energy, Via Lambruschini 4a, 20156 Milano, Italy

ARTICLE INFO

Article history:
Received 11 June 2015
Received in revised form 11 October 2015
Accepted 30 November 2015
Available online 14 December 2015

Keywords:
Bubbly flow
Annular gap
Bubble diameter distribution
Bubble shape
Flow regime transition
Counter-current flow

ABSTRACT

An understanding of the bubble properties, size distributions and shapes is of fundamental importance for comprehending flow dynamics and mass transfer phenomena in bubble column reactors. A large number of studies have focused on open tube bubble columns, and the knowledge concerning bubble columns with internals is still limited. This paper contributes to the existing discussion experimentally investigating a counter-current annular bubble column with 0.24 m inner diameter and two internal pipes. The experimental investigation consists in holdup measurements and image analysis. The former is used for identifying the flow regime transition and studying the bubble column hydrodynamics, whereas the latter is used for investigating the bubble shapes and size distributions. The definition of the transition point is important because the size distribution and bubble shapes depend on the operating conditions and a change of the bubble properties is expected near the transition. The image analysis is applied at different superficial gas and liquid velocities, corresponding to a gas holdup between 2.9% and 9.6%. It is difficult to measure bubble size distribution accurately in large-diameter bubble columns owing to the overlapping of bubbles, even at low void fractions, and—in an annular gap bubble column—the fact that cap bubbles have also been reported in the homogeneous flow regime. The use of a bubble image analysis method to study the bubbly flows in a large-diameter annular gap bubble column is described. In the proposed method, each bubble is approximated and reconstructed using an ellipse. The proposed approach is used to quantify the bubble size distribution, as well as to study the bubble shape and orientation as function of the superficial gas and liquid velocities. The experimental data obtained are used to develop a correlation between non-dimensional parameters and aspect ratios. Also, the experimental data are compared with non-dimensional diagrams from the literature, revealing good agreement. Finally, the image analysis is used for supporting the flow regime transition prediction in the stability analysis method: the virtual mass formulation is obtained by using the aspect ratio correlation provided by the image analysis. The stability analysis—supported by the image analysis—was able to predict the transition point in very good agreement with experimental data and performed better than literature correlations.

1. Introduction

Gas–liquid flow in vertical pipes and bubble columns is encountered at several plants in the chemical, energy and nuclear fields. The correct design and operation of these devices relies on the proper prediction of the flow pattern and the flow properties. In particular, the gas holdup, ε_G, and the bubble diameter, d_b, (obtained from the bubble size distribution, BSD) allow the evaluation of the interfacial area, a_i, for the evaluation of the heat and mass transfer rate. The value of the gas holdup and the bubble size distribution depend upon the superficial gas velocity U_G and is related to the prevailing flow regime: mainly, the homogeneous and the heterogeneous regime [1]. The former is associated with small gas superficial velocities and is characterized by the presence of small, uniform-sized bubbles with little interactions. The latter is associated with high gas superficial velocities, high coalescence and breakage phenomena and a wide variety of bubble sizes. The transition from the homogeneous regime to heterogeneous regime is a gradual process in which a transition flow regime occurs. This flow regime is characterized by large flow macro-structures with large eddies and widened bubble size distribution due to the onset of bubble coalescence. The global and the local flow properties are not only influenced by the flow regime but also by the bubble column operation. Bubble columns can be operated in the co-current, counter-current or semi-batch mode. Whereas the co-current or semi-batch modes are widely studied, the counter-current mode

* Corresponding author. Tel.: +39 02 2399 3826.
E-mail addresses: giorgio.besagni@polimi.it (G. Besagni), fabio.inzoli@polimi.it (F. Inzoli).

http://dx.doi.org/10.1016/j.expthermflusci.2015.11.020
0894-1777/

Nomenclature

Non-dimensional numbers

$Bo = \frac{\rho_L g d_{eq}^2}{\sigma}$ bond number (–)

$Eo = \frac{g(\rho_L - \rho_G) d_{eq}^2}{\sigma}$ Eötvös number (–)

$Fr = \frac{v^2}{g d_{eq}}$ Froude number (–)

$Ga = \frac{\rho_L g^{1/2} d_{eq}^{3/2}}{\mu_L}$ Galilei number (–)

$M = \frac{g(\rho_L - \rho_G)\mu_L^4}{\rho_L^2 \sigma^3}$ Morton number (–)

$Re = \frac{\rho_L v d_{eq}}{\mu_L}$ Reynolds number (–)

$We = \frac{d_{eq} v^2 \rho_L}{\sigma}$ Weber number (–)

Acronyms

BSD	bubble size distribution
CFD	computational fluid dynamics

Symbols

a	major axis of the bubble (m)
b	minor axis of the bubble (m)
c	coefficient in the ellipse equation (–)
α	coefficient in the aspect ratio correlation (–)
A^*, B^*	parameter in the Reilly correlation for the flow regime tranistion (–)
A, B, C, F, G, Z, β_0, β_0'	coefficients in the stability analysis (–)
C_V	virtual mass coefficient (–)
d_{holes}	gas sparger holes diameter (mm)
d_c	diameter of the column (m)
d_{eq}	bubble equivalent diameter (m)
d_b	bubble diameter in the stability analysis formulation (m)
D_H^*	non-dimensional diameter (–)
$D_{H,Cr}{}^*$	critical non-dimensional diameter (–)
f	parameter for the evaluation of the flow regime in the stability analysis (–)
H_c	height of the column (m)
H_D	heights of the free-surface after aeration (m\)
H_0	heights of the free-surface before aeration (m)
J	drift flux (m/s)
g	Gravity acceleration (m/s^2)
S	*parameter in the swarm velocity method* (–)
x	horizontal axis (–)
x_c	horizontal coordinate of the bubble center (m)
y	vertical axis (–)
y_c	vertical coordinate of the bubble center (m)
u_∞	terminal bubble rise velocity (m/s)
U	superficial velocity (m/s)
v	bubble velocity (m/s)
ϑ	bubble orientation (∘)
μ	dynamic viscosity (Pa s)
σ	surface tension (N/m)
φ	aspect ratio (–)
WE_{cr}	critical Weber number (–)
ε_G	gas holdup (–)

Subscripts

L	liquid phase
G	gas phase
T, E	subscripts in the drift flux formulation
trans	transition point
exp	experimental data
swarm	swarm velocity

is by far less investigated, as also point out in the review of Leonard et al. [2].

Among the broader framework of two-phase flow, this paper investigates a counter-current large-diameter pipe with two inner tubes. The bubble column is $d_c = 0.24$ m inner diameter, $H_c = 5$ m height, the air is introduced up to $U_G = 0.2$ m/s and the water is recirculated up to $U_L = -0.11$ m/s. Vertical pipes with inner tubes are described in the literature concerning annular bubble columns or vertical annuli channels. Bubble columns are frequently studied without considering internal tubes, but annular gap configurations can occur in internal-loop, air-lift bubble columns, photo-catalytic bubble column reactors containing lamps positioned on their centerlines and in heat exchangers (i.e., the reader may refer to the review of Youssef et al. [3]). Annular channels are widely studied because they may replicate certain of the phenomena found in complex geometries, such as in in separators, fuel bundles and steam generators. When considering bubble columns and vertical pipes, an important parameter is the pipe diameter. The pipe considered in this study is a large-diameter pipe, under ambient operating conditions, on the basis of the dimensionless diameter $D_H{}^*$ proposed by Kataoka and Ishii [4]:

$$D_H^* = \frac{D_H}{\sqrt{\sigma / g(\rho_L - \rho_G)}} \quad (1)$$

where D_H is the hydraulic diameter, σ is the surface tension coefficient, g is the gravity acceleration and $\rho_L - \rho_G$ is the density difference between the two phases. Pipes with dimensionless diameters greater than a critical value $D_{H,cr}{}^* = 52$ are considered to be large-diameter pipes [5]. Considering air and water at atmospheric conditions, the critical hydraulic diameter is $D_{H,cr} \approx 0.13$ m. When the pipe diameter is larger than such a value, the stabilizing effect of the channel wall on the interface of the Taylor bubbles becomes lower and the slug flow can no longer be sustained due to Rayleigh–Taylor instabilities. The hydrodynamics in large pipes differs from flow in small pipes because of changes in the liquid field around the bubbles, presence of additional turbulence and strong secondary recirculation [6]. Therefore, the experimental data—i.e., bubble size distribution (BSD)—and models for small pipes—i.e. for the flow regime transitions—cannot be scaled up to develop an understanding of the flow in large pipes. Our experimental facility has a dimensionless diameter of $D_H{}^* = 88.13$, without considering the internal pipes, and $D_H{}^* = 47.37$ in the annular gap configuration. Such values are higher than the ones commonly investigated in the literature and the present experimental setup differs from the ones previously investigated, as deeply discussed in literature survey proposed by Besagni et al. [7]. For these reasons, ad-hoc experimental campaigns (i.e., for obtaining gas holdup, bubble size distributions and local flow properties) must be performed. The very first experimental results of the present annular gap configuration have been presented by Besagni et al. [7,8] and were used for assessing a Computational Fluid-Dynamic model [7]. Despite the previous investigations, some open unsolved issues remain, especially if concerning the bubble shape and BSDs.

The knowledge of the BSD is of fundamental importance for the correct design and modeling of a chemical reactor. Indeed, the BSD—together with the gas holdup—enables the computation of the interfacial area (the main parameter for the evaluation of heat and mass transfer at the interface). Furthermore, the BSD should be also provided to set-up a Computational Fluid Dynamics (CFD) model: an Eulerian two-fluid approach requires BSD information

as an input and for the interfacial closures. In the literature, there is a lack of studies concerning BSD in annular gap bubble columns and annulus channels [3]; also, the influence of the liquid velocity on the bubble shape and bubble size distribution is far from being understood and there is a lack of literature on this topic [9]. On the other hand, other systems have been widely studied in the literature. Generally speaking, various intrusive and non-intrusive techniques can be used for measuring BSD and describing bubble shapes [10–12]. Non-intrusive measurements techniques are preferred over intrusive methods—i.e., optical probes [13,14]—because the flow conditions are not disturbed, and image analysis is attracting increasing attention owing to the many advantages it offers. One method for obtaining bubble information from a digital image is to manually draw lines on in-focus bubbles and then use a code to measure those lines [15,16]. This technique does not require the development of an image-processing algorithm but is time consuming and also introduces uncertainty owing to the subjectivity of the method. Shepard [17] compared the results of the line drawing technique from six different users for an identical set of images: the average bubble diameter could vary by ±5%, and the bubble diameter standard deviation could vary by ±3%. Another approach is to use image-processing algorithms. However, these techniques are still limited to resolve large bubble clusters, highly unsteady flows and large void fractions [18]. Additionally, at low gas holdup, there are problems associated with overlapping: if the gas holdup exceeds 1%, more than 40% of the bubbles are overlapping in the image [19,20]. Various studies have addressed this problem and have proposed different methods for dealing with overlapping bubbles [21]; however, no agreement has been found, and some approaches may cause a significant reduction of the bubble sample size and an underestimation of the bubble diameter. Most of the studies focus on rectangular and small scale [21–23] or medium scale [24] bubble columns. It is, in fact, difficult to accurately measure BSD in large-diameter bubble columns owing to the overlapping of bubbles on different planes and—in annular gap bubble columns—cap bubbles have also been reported in the homogeneous flow [8]. The proposed study investigate the bubble shape and BSD in the counter-current configuration in order to extend the available dataset and provide further information for the design and modeling of bubble column reactors.

When discussion the BSD, the definition of the flow regime transition is of fundamental importance. Indeed, the BSD and bubble properties are also a function of the operating condition and a change of the bubble properties is expected near the flow regime transition. In the literature, a large number of authors have studied the flow regime transitions in open tube bubble columns; however, from the review of Shaikh and Al-Dahhan [25] and Nedeltchev and Shaikh [26], is it clear that firmly established criteria are not yet available. Furthermore, studies concerning annular gap configurations are still rare and the methods proposed for the open tube configurations should be evaluated also for the annular gap bubble column. In our previous works, we have investigated the flow regime transition using the Swarm velocity method only [7,27]. In the present paper, we improve the evaluation of the flow regime transition by also applying the Wallis method [28] and by the linear stability analysis [29–34]. In the stability analysis approach, the equations for continuity and motion for or gas–liquid dispersions are written and combined, then, perturbations are introduced and the resulting equations are linearized. In the homogeneous regime, any perturbation decays with respect to time. In contrast, if the small perturbations grow with time, transition to the heterogeneous regime occurs. In the mathematical formulation of the approach, the virtual mass and the diffusion coefficients appear [29]. In particular, the virtual mass coefficient depends on the bubble shape and suitable correlations for the aspect ratio should be used. Most of the correlations available in the literature have been derived for single droplets/bubbles and their use for bubbly flow may be questionable. In this paper, we solve this issue by coupling the stability analysis along with the image analysis and we propose a suitable correlation for bubble flows, on the basis of the experimental data obtained.

Taking into account the literature survey, the general aim of this paper is to provide a better understanding of the two-phase flow phenomena in a counter-current annular gap bubble columns, through an experimental investigation consisting in holdup measurements and image analysis. The holdup measurements are used for describing the global hydrodynamic and for investigating the flow regime transition. After the flow regime transition has been identified, the image analysis is used for quantify the bubble size distributions and to study the bubble shapes, as function of the superficial gas and water velocities. The obtained data provide an insight in the columntwo-phase flow, enhance the reactor design comprehension and can be used for supporting numerical studies. Another outcome of this paper is the discussion of the relationship between the bubble size (and non-dimensional numbers) and the aspect ratio in bubbly flows, whereas the previous literature discussed only these relations for single rising bubbles. A correlation between the Eotvos number and the aspect ratio is proposed and is used for supporting the stability analysis—inside the formulation of the virtual mass coefficient—in the estimation of the transition point. The results of the proposed approach are very good agreement with experimental data and the proposed method performed better than the literature correlations.

The paper is structured as follows. In Section 2, the experimental setup is explained and the measurement techniques are detailed. In Section 3, the main experimental results are summarized and the aspect ratio correlation is presented. In Section 4, the stability analysis is applied, the results are discussed and sensitivity analysis concerning the dispersion coefficient and the virtual mass formulation are presented. Finally, results are summarized and conclusions are given.

2. Experimental setup and method

2.1. Experimental setup

The experimental facility is a non-pressurized vertical pipe made of Plexiglas with $d_c = 0.24$ m and $H_c = 5.3$ m (Fig. 1a and b). Two internal PVC pipes are positioned—one centrally positioned (with an external diameter of 60 mm) and one asymmetrically positioned (with an external diameter of 75 mm). The air is introduced up to a superficial gas velocity up of $U_G = 0.2$ m/s and the water is recirculated up to $U_L = -0.011$ m/s. The air distributor, which is positioned asymmetrically, comprises a stainless steel tube with an external diameter of 70 mm, a height of 340 mm and holes positioned along the circumference with diameters $d_{holes} = 3.5$ mm (Fig. 1c). A pressure reducer controls the pressure upstream from the rotameters (1) and (2), used to measure the air flow rate. A pump, controlled by a by-pass valve, provides water recirculation, and a rotameter (3) measures the water flow rate. The uncertainty in the evaluation of the mass flows may be found in Table 1. Clean filtered deionized water was used, and the air and water temperatures were maintained at room temperature (22 ± 1 °C) during the experiments. Further information on the experimental facility may be found in the dissertation of Carrara [35].

The values of gas density (used to compute the superficial gas velocity) are based upon the operating conditions existing at the column mid-point. The mid-point column pressure was assumed to be equal to the column outlet pressure plus one-half the total experimental hydrostatic pressure head. The mid-point column

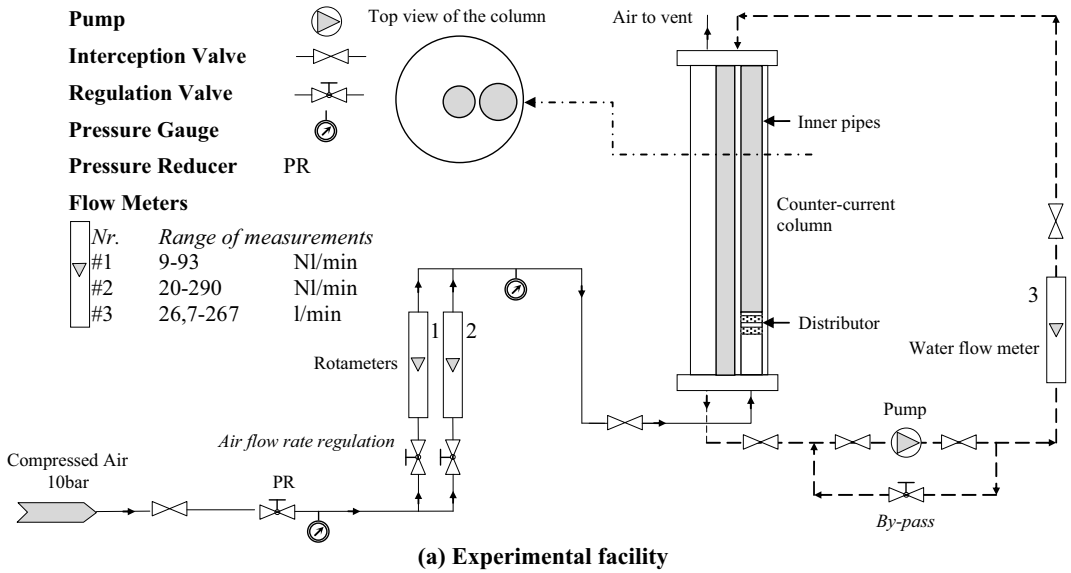

(a) Experimental facility

(b) Photo of the facility

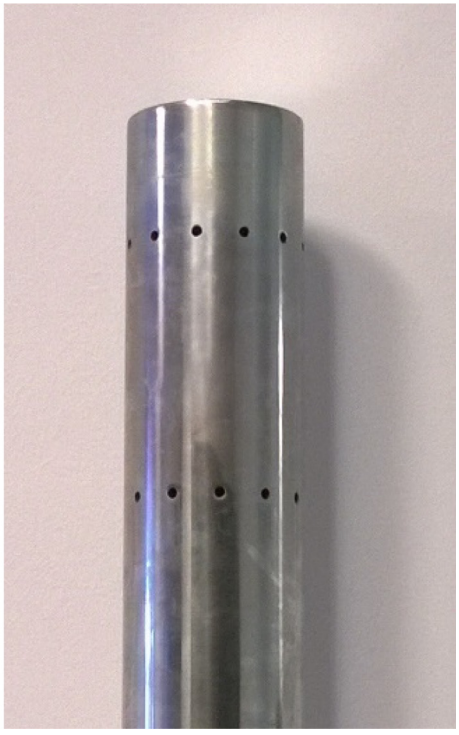

(c) Air distributor

Fig. 1. Experimental facility.

Table 1
Accuracy of measurement devices.

Measurement device	Accuracy (%)[a]
Air flow rates	2
Water flow rate	1.5

[a] f.s.v.

pressure was assumed to be equal to the column outlet pressure plus one-half the total experimental hydrostatic pressure head.

It is worth noting that the diameter of the column, its height and the distributor openings were chosen considering the well known scale up criteria reported in the literature: generally a diameter greater than 0.15 m, an aspect ratio larger than 5 and distributor openings larger than 1.5 mm guarantee results that could be used for scaling up [1,2].

2.2. Holdup

2.2.1. Holdup measurements

Measurements of the bed expansion allowed the evaluation of the gas holdup ε_G. The procedure involves measuring the location (height) of liquid free surface when air flows in the column:

$$\varepsilon_G = \frac{(H_D - H_0)}{H_0} \tag{2}$$

where H_D and H_0 are the heights of the free-surface after and before aeration, respectively.

2.2.2. Flow regime transition analysis

The holdup measurements are used for evaluating the flow regime transition point using two methods from the literature.

2.2.2.1. Swarm velocity method. The first method is the one developed by Zuber and Findlay [27] based on the swarm velocity:

$$U_{swarm} = U_G/\varepsilon_G \tag{3}$$

The swarm velocity is plotted against the superficial gas velocity: U_{swarm} is constant in the homogeneous regime but begins to increase as the system enters the heterogeneous regime at a certain transition superficial velocity U_{trans}. The appearance of the first large bubble is responsible for this sudden increase in swarm velocity and is an indication of flow regime transition. In this study, the quantitative evaluation of U_{trans} is determined by the intersection between the trends of U_{swarm} in the two regimes. U_{swarm} is constant for the homogeneous regime:

$$U_{swarm,bubbly\ regime} = constant \tag{4}$$

where as in the transition flow regime, it is determined by a least squares fitting of the following function:

$$U_{swarm,transition\ regime} = S_1(U_G)^{S_2} + S_3 \tag{5}$$

where S_1, S_2 and S_3 are fitting parameters. The transitional velocity is then evaluated by solving the following equation:

$$U_{swarm,bubbly\ regime} = U_{swarm,transition\ regime} \tag{6}$$

2.2.2.2. Wallis plot method. The second method is the drift-flux plot proposed by Wallis [28]. This method is based on the drift flux, which represents the gas flux through a surface moving with the speed of the two-phase mixture and is experimentally obtained as follows:

$$J_T = U_G(1-\varepsilon_G) \pm U_L\varepsilon_G \tag{7}$$

which for a null water velocity, reads as follows:

$$J_T = U_G(1-\varepsilon_G) \tag{8}$$

for a counter-current flow, reads:

$$J_T = U_G(1-\varepsilon_G) - U_L\varepsilon_G \tag{9}$$

Theoretically, the drift flux is written in terms of the bubble swarm velocity, whose dependedcf7u8po8l ùnce upon ε_G varies with the prevailing regime:

$$J_E = U_b(1-\varepsilon_G) \tag{10}$$

The idea in this method is to employ a model for U_b that is valid for the homogeneous regime, plotting J_E and J_T in the same graph as a function of ε_G. In the homogeneous regime, J_E is equal to J_T, and the transition point is defined when:

$$J_T \neq J_E \tag{11}$$

The evaluation of U_{swarm} is a matter of discussion in the literature, and different models have been proposed and applied. In this study, we follow the approach of Krishna et al. [36], which is based on the empirical model of Richardson and Zaki [37]:

$$U_b = u_\infty(1-\varepsilon_G)^{n-1} \tag{12}$$

where n is fluid-dependent ($n \cong 2$ for water) and u_∞ is the terminal velocity of an isolated bubble, which should be fitted with the aid of the experimental data, in the determination of the regime transition point. From Eqs. (10) and (12), we obtain the following:

$$J_E = u_\infty\varepsilon_G(1-\varepsilon_G)^n \tag{13}$$

2.3. Flow visualization

2.3.1. Instrumentation

The photos were taken using a Canon α200 camera (1/1200s, ISO400, f/3.5) in the developed region of the two-phase flow approximately 2.4 m above the air distributor. The backlight method is employed in the experiments, and the light source is a 500 W halogen lamp. The resolution of the images is approximately 3872 × 2592 pixels. Visualization sections consist of square boxes (filled with water) around the vertical pipe designed for correcting the distorted image. Even if the test section is covered by the square box filled with water, some refraction problem may remain, as the refraction index of pipe wall is different from that of water. Indeed, the refractive index of the plexiglass is 1.48 and the one of water is 1.33. However, this effect is negligible: indeed, if considering the two inner pipes used as reference for the pixel/mm conversion (please refer to the next Section), the conversion factor is 12.12 pixel/mm for the central pipe and 12.29 pixel/mm for the lateral pipe. The difference between the two values is about 1.5%. A difference 0.17 pixel/mm is negligible if we consider that there is an uncertainty of, at least, 1 pixel in the selection of the points for detecting the bubbles edge. A complete discussion of the visualization section, the distortion problems and the design of the visualization sections may be found in the dissertation of Carrara [35].

2.3.2. Image analysis method

The goal of the image analysis approach is to obtain bubble information concerning bubble shape, bubble orientation and diameter distribution. The image analysis is based on the bubble sampling approach proposed by Aloufi [38] for a small-diameter bubble column. In this approach, each bubble is approximated and reconstructed using an ellipse (Fig. 2), represented by the following equation:

$$c_1x^2 + c_2xy + c_3y^2 + c_4x + c_5x + 1 = 0 \tag{14}$$

The method is structured in three phases:

1. *Calibration:* The reference conversion factor between pixels and millimeters is provided.
2. *Bubble reconstruction:* For each bubble, six points on the bubble are selected (by human vision), and ellipse equation parameters c_1, c_2, c_3, c_4 and c_5 are evaluated using the least square method.
3. *Bubble processing:* The equivalent ellipse is processed to obtain the major axis $2a$, the minor axis $2b$, the center of the bubble x_c e y_c and the orientation angle θ (Fig. 2). Finally, the bubble equivalent diameter d_{eq} and aspect ratio φ are obtained:

$$d_{eq} = 2\sqrt[3]{a^2b} \tag{15}$$

$$\varphi = \frac{b}{a} \tag{16}$$

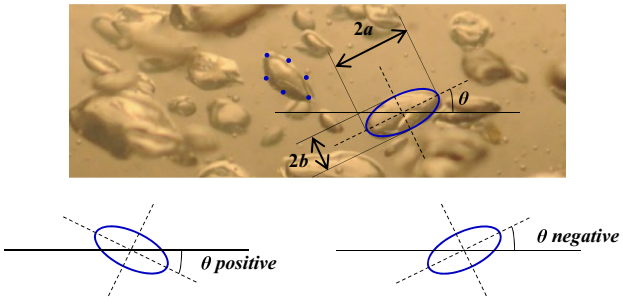

Fig. 2. Image processing.

The focus of the camera was adjusted on the external diameter of the inner pipes (the midplane of the column). This value is then used for the correction to the real size of the bubbles. Of course, an uncertainty exists in adjusting the focus of the camera on the column midplane; therefore, we have selected a region in which all of the bubbles can be considered at the same focal distance as the external diameter of the pipes. The definition of this region is very important and is be selected in order to avoid loss of information. This region is defined by a line at a distance x from the center of the column (Fig. 3). In general, for the choice of the value of x, two factors have been taken into account:

(a) With increasing x, the area of interest decreased and the bubbles were closer to the reference plane, thus reducing the error.
(b) With increasing x, the number of bubbles to be analyzed decreased.

After a sensitivity analysis, the value $x = 0.3\ d_c$ was used and the corresponding area is colored gray in the schematic drawing of the column in the Fig. 3a. The sensitivity analysis was conducted as follows:

(1) a complete image was sampled.
(2) x between 0.1 d_c and 0.5 d_c was considered.
(3) the different bubble parameter were analyzed for the different positions.

For $x < 0.20\ d_c$, the number of bubbles sampled decreased considerably because of the small region, whereas, for $x > 0.25$ the bubble parameters did not change increasing x. For $x > 0.35\ d_c$, the number of in-focus bubbles decreased because of the higher overlapping As a results, $x = 0.3\ d_c$ was found to provide satisfiable results and was considered in the following of the study. Furthermore, Besagni et al. [7] proved that the BSD obtained in this area—for a single operating condition—allows the correct modeling of the column in the Eulerian–Eulerian framework. Therefore, we may assume that the BSD obtained are representative of the bubble size distribution in the column.The selected was also divided into four zones to study the bubble shape and BSD at various distances from the wall (Fig. 3b). The four zones were chosen to have the same width equal to 0.075 d_c.

The number of bubbles to be sampled to achieve a reliable BSD is a matter of discussion in the literature [39]. Various studies have sampled different numbers of bubbles—between 50 and 100 [40], 200 [41], 250 [42], 300 [43], between 250 and 300 [38] and 100 [44]. In this study, at first, $U_G = 0.0037$ m/s – $U_L = 0$ m/s was considered and 2590 bubbles were selected using 32 photos taken over a period of 1000 s to obtain time-averaged results. Then, an analysis concerning the number of bubbles sampled to achieve a reliable BSD was performed and can be found in Appendix A. Taking into account that, at least, 400 bubbles should be sampled to achieve a reliable BSD (Appendix A), about 800–1000 bubbles were sampled for the other operating conditions. The number of bubbles sampled for every photo was the maximum number of bubbles detected in the selected region. The number of bubbles was between 50, for the lower superficial gas velocity conditions, and 200, for the higher superficial gas velocities.

Of course, the approach used has some limitations. At first, the test section is not symmetric and a limited area was considered in the image analysis. However, the results and BSD obtained may be considered realistic and represent the BSD in the column: this is proved if considering the experimental and numerical investigation proposed by Besagni et al. [7] where the BSD obtained for a single operating condition allowed the correct modeling of the column in the Eulerian–Eulerian framework. It is, indeed, well known the sensitivity of the Eulerian–Eulerian approach to the bubble size and a wrong input BSD would result in wrong results [7,45–47]. Another consideration is devoted to the overlapped images: the number of sampling point used for obtaining the equivalent ellipse were more than the minimum number of points for defining an ellipse (five points): this allows sampling the bubbles also in overlapping conditions. Therefore, the BSD obtained may be considered realistic and represent the BSD in the column.

The other limitation of this approach is that only projected bubble image can be obtained in this experiment and, in this case, accurate measurement of bubble shape and bubble orientation is – of course- not possible. This problem is well known in the literature and, despite some proposals [48,49], this problem is far from being solved and the use of 2D projected images is a common way of processing the bubble images (refer, for example, to [18,21,23,40,41]. The investigation of this uncertainty is a matter of future discussion. However, the bubble shape data obtained in this approach are considered reliable: as will be discussed in the Section 4, the bubble shape information obtained allows the extrapolation of correlations for the aspect ratio and method for the flow transition analysis. The results of the analysis were in agreement with the experimental data and, therefore, the bubble shape information are considered reliable.

Finally, if considering the approximation of bubbles with ellipses, Lage and Espósito [40] stated that the error in the measurement of each axis of the ellipse is equal to about 6%. Considering the error introduced by the hypothesis of oblate spheroid and the optical distortion, they estimated that the experimental error in the determination of the equivalent diameter is between 10 and 15%. In the present case, the reader should refer to Appendix

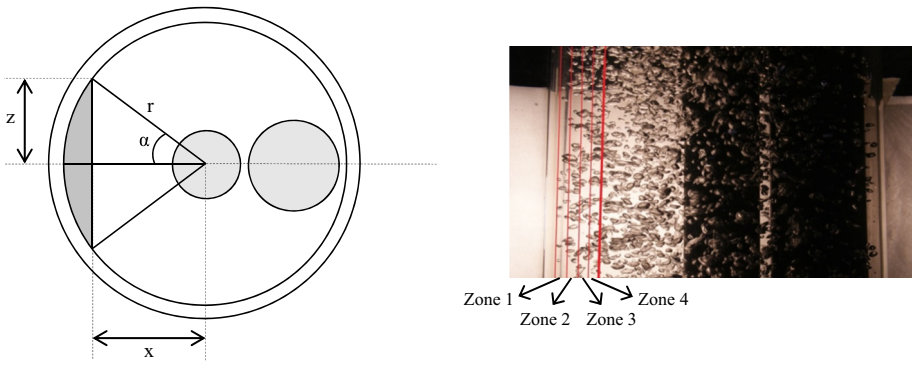

(a) Top view of the column **(b) $U_G = 0.0087$ m/s**

Fig. 3. Layout of the system.

B for analysis concerning the errors made during the bubble shape estimation due to the handpicked points.

3. The experimental results

Herein, the experimental results are presented and discussed. The holdup measurements are used for investigating the flow regimes and identifying the bubbly flow regime transition. Once the bubbly flow transition has been detected, the bubble image analysis is applied for providing an insight in bubble properties.

3.1. Gas holdup

3.1.1. Gas holdup measurements

The gas holdup measurements are shown in Fig. 4 for the different superficial water velocities. The slope of the holdup curves is the one typically found for similar sparger geometries. Indeed, it is known from the literature that the shape of the holdup curve mainly depends upon the distributor used and the diameter of the distributor openings [50]. The distributor used has "large" openings (d_{holes} > 1 mm) and the shape of the holdup curve is the one typically obtained for distributor with similar openings (i.e., single/multiple nozzles, spider sparger or perforated plate distributors with hole diameter greater than 1 mm); moreover, as expected, no peak can be observed in the holdup curve. At low superficial air velocity, in the bubbly flow regime, the relation between the gas holdup and the air superficial velocity is linear, followed by a change in slope due to the flow regime transition. In this region, the slope of curve changes continuously, indicating a continuous increase of the large bubble component [50] (as also verified in the image analysis, Section 3.2.2). Considering the studies proposed by Nedeltchev [51] we may state that the homogeneous regime could be considered as a maldistribution flow regime due to the large opening of the holds in the distributor. By increasing the liquid flow rate, a faster increase in the holdup is observed at low superficial gas velocities and the transition point moves toward lower superficial gas velocities, as explained in Section 3.2. Above the transition velocity, large deformed bubbles start to appear (as also verified in the image analysis, Section 3.2.3), and the bubble coalescence increases the average rise velocity and reduces the gas residence time in the column, hence decreasing the gas holdup versus gas velocity slope. Above $\varepsilon_G \approx 16$–17%, the superficial water velocity has no more and influence on the holdup. The discrepancy of the holdup in the transition regime between the no liquid flow and the countercurrent configurations is hardly justified, despite a possible explanation was proposed by Besagni et al. [7].

In the literature, Otake et al. [52] observed an increase in the holdup and earlier regime transitions as the countercurrent liquid flow rate is increased in a small pipe with a diameter of 005 m. Their analysis covered gas superficial velocities up to 00,824 m/s and liquid superficial velocities up to −0.15 m/s. Similar conclusions were drawn by Yamaguchi and Yamazaki [53] for small pipes with diameters of 004 m and 008 m, with gas superficial velocities up to 1 m/s. On the contrary, Akita and Yoshida [54] observed that the liquid flow rate had no influence in a large pipe with a diameter of 0152 m at gas superficial velocities up to 0032 m/s and liquid superficial velocities up to 004 m/s. The latter is in disagreement with what we observed in the bubbly flow regime, while the formers suggest an influence of liquid flow rate at gas superficial velocities higher than 006 m/s. A comprehensive comparison with previously published experimental data and correlations from the literature was proposed by Besagni et al. [7].

3.1.2. Flow regime transition

The flow regime transition has been investigated by using the methods presented in Section 2.2.2. Fig. 5a presents the swarm velocity plot: as expected the swarm velocity is constant in the homogeneous regime, but it starts to increase as the system enters the transition flow regime. Fig. 5a represents a close view of the transition point by using the Swarm velocity method—Eq. (6)—and Fig. 6 evaluates the transition point using the Wallis plot. The value of the U_{trans} obtained with the two methods are in

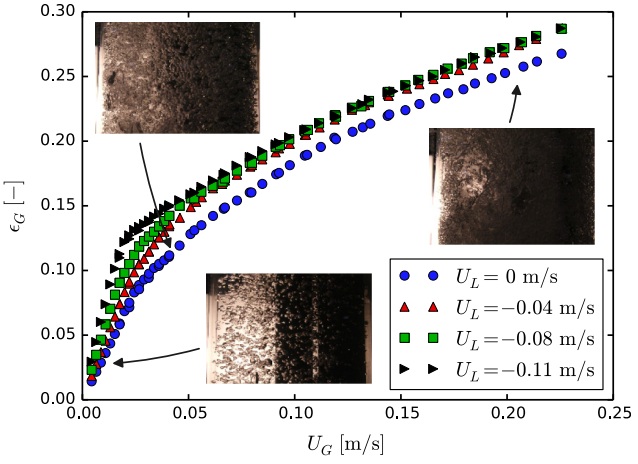

Fig. 4. Holdup measurements.

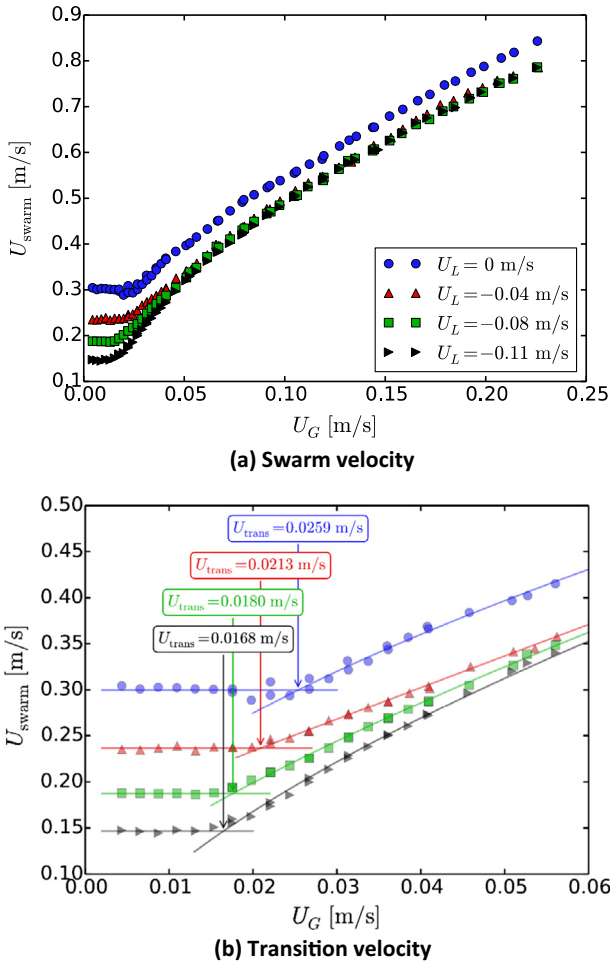

Fig. 5. The swarm velocity method for the flow regime transition evaluation.

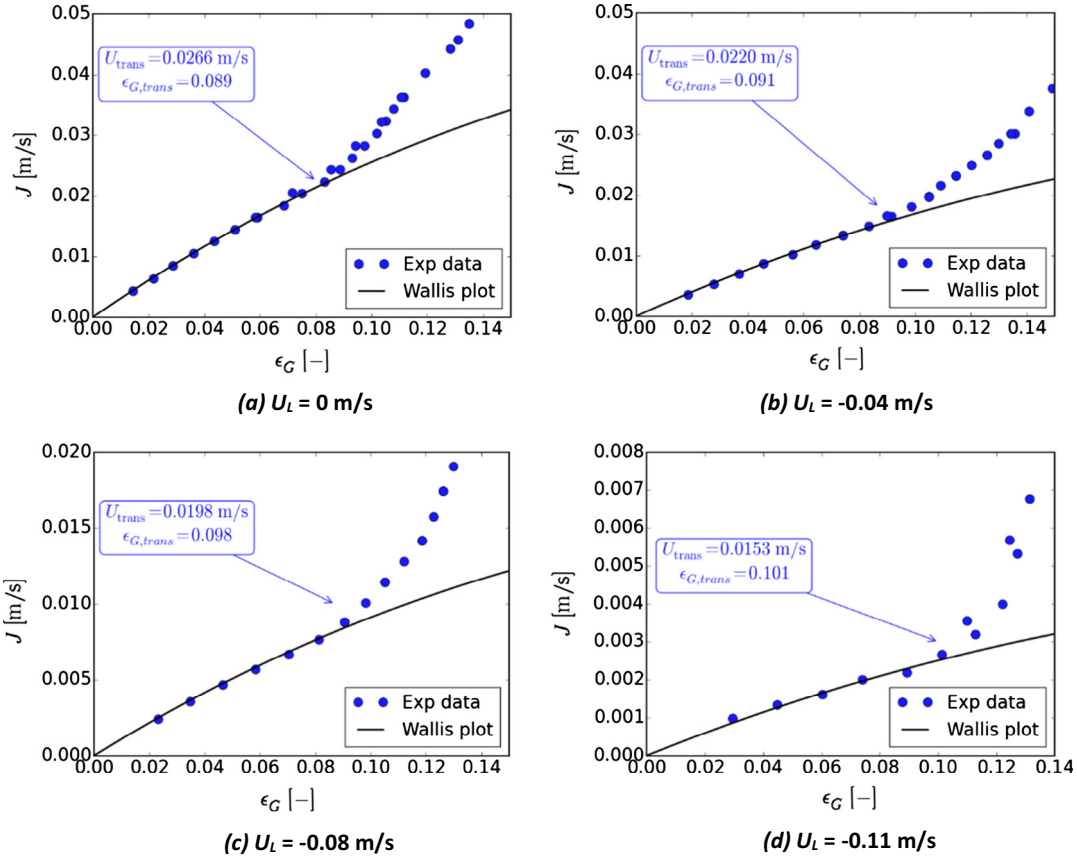

Fig. 6. The drift flux method for the flow regime transition evaluation.

agreement and, following the proposal of Ribeiro and Mewes [55], the transition point have been evaluated as the mean of the two values. U_{trans}, depending on the liquid velocity, lie in the range between 0.0263 m/s and 0.0161 m/s (Table 2). U_{trans} decreases while increasing the liquid velocity: the counter-current operating conditions destabilize the homogeneous flow. Indeed, the counter-current liquid slows the bubbles and increase the holdup; thus, for the same superficial gas velocity, the mean distance between the bubbles decreases, and therefore, coalescence phenomena may occur more easily because of the expected increase in bubble collisions [7]. Comparing our transition point with the literature data, attention should be given to the distributor. Following the discussion of Besagni et al. [7], the distributor may be classified into "coarse" and "fine" distributor. Single and multiple nozzles or perforated plate distributors with hole diameter greater than 1 mm ("coarse" distributors) usually lead to an early regime transition, while "fine" distributors such as porous plates [56,57] or needles [58] can maintain a stable bubbly flow at higher gas flow rates. The distributor considered in this study is of the "coarse" type. Therefore, the flow regime transition is found to occur early is compared to fine distributor: due to the large diameter of the holes in the distributor, large bubbles with a consequent break up phenomena and a change in bubble size distribution appears in the near sparger region. In particular, our values of U_{trans} are in agreement with the studies of Dargar and Macchi [59], Rollbusch et al. [60], Nedeltchev and Shaikh [26], Zahradnik and Fialova [61] and Besagni and Inzoli [62].

3.2. Image analysis

After the flow regime transition was detected, the image analysis may be used for investigating the bubble properties in the homogeneous flow. In particular, in this paper, we focus analyze the operating conditions listed in Table 3. The operating conditions were selected taking into account the followings:

- influence of U_G in the homogeneous flow and after the flow regime transition.
- influence of U_L in the homogeneous flow.

3.2.1. Homogeneous flow regime

In this section, we propose a qualitative description of the homogenous flow regime. In particular, we focus on the U_G = 0.0087 m/s condition, without the loss of generality. In this flow regime, some bubbles were spherical (Fig. 4a and b), others

Table 2
Flow regime transition points.

U_L (m/s)	$U_{G,trans}$ (m/s)	$\varepsilon_{G,trans}$ (−)
0	0.0263	0.0874
−0.04	0.0217	0.09074
−0.08	0.0189	0.09714
−0.11	0.0161	0.1077

Table 3
Operating conditions investigated by using the image analysis.

U_G (m/s)	U_L (m/s)	ε_G (%)
0.0087	0	2.89
0.0220	0	7.51
0.0313	0	9.75
0.0087	−0.04	3.62

were ellipsoidal (Fig. 7c and d), and others were irregular in shape (Fig. 7e, g, f, h); around the inner pipes, large cap-bubbles periodically appeared (Fig. 7j and i). The cap-bubbles seemed to originate around the inner pipes where the flow recirculation phenomena occurred. These recirculation phenomena were particularly intense in the space between the external pipe and the wall of the column. The cap bubbles raised the column at a higher velocity compared to the other bubbles; they dragged swarms of smaller bubbles in their wake and generated break-up phenomena in the path. Owing to the presence of the cap-bubbles, this regime can be better defined as a pseudo-homogeneous regime. Moving away from the central pipe toward the column wall, the bubbles were mostly uniformly distributed in the cross-section of the pipe [7], traveling vertically with minor transverse and axial oscillations. During the image analysis of this condition, we detected 388 bubbles in zone 1,917 bubbles in zone 2,855 bubbles in zone 3 and 430 bubbles in zone 4. The number of bubbles in area 4 decreased compared to zone 3 owing to the appearance of the cap-bubbles, leading to more overlapping of bubbles. The interested reader may refer to the study of Besagni et al. [7] for flow visualizations of other superficial gas velocities (after the flow regime transition) and the influence of the superficial water velocity.

3.2.2. Bubble size distributions

Figs. 8a and 9a show the average distribution of the equivalent diameters of the bubbles for the different superficial gas and water velocity, respectively. The bubble diameter distribution is detailed by using histograms with 26 classes. Each class has an extension of 0.5 mm.

Considering U_G = 0.0087 m/s, the BSD is bimodal: the first peak of frequency appears between 0.5 and 1 mm and the second between 3 and 3.5 mm. The presence of two maxima is also noticed in the distribution of the equivalent diameters in each individual photograph. Increasing the superficial gas velocity, the number of small bubbles decrease and the second peak moves toward higher bubble diameters. In particular, after the flow regime transition (considering U_G = 0.0313 m/s), the BSD is considerably different from the other BSDs, being shifted toward higher bubble diameters. This is in agreement with the studies concerning the size of the bubbles and the flow regime transition [63]. Increasing the superficial water velocity, the BSD moves toward higher bubble diameter. In particular, the first peak of frequency moves from 0.5–1 mm toward 1–1.5 mm and the second peak of frequency moves from 3–3.5 mm toward 4.5–5 mm. A bimodal distribution has also been found in the literature [21,41,64,65]. In particular, Lau et al. [21] and Wongsuchoto et al. [41] observed a transition from unimodal distribution to bimodal distribution with increasing superficial velocity of the air. This change in the distribution of bubble size has been justified with increased coalescence [21] or break-up [41], and—as mentioned previously—in the annular gap configuration, coalescence and break-up occurs at low gas flow rates owing to the presence of the large cap-bubbles. Indeed, the passage of the cap-bubbles causes local recirculation, high turbulence, rupture of bubbles and the entrainment of small bubbles. For this configuration of the column, photographs are not available at a lower gas flow rate, and it is therefore impossible to compare the BSDs to verify the passage from unimodal distribution to bimodal distribution. It is interesting that—even near the wall—the BSD was not unimodal. This may suggest that smaller bubbles may have been pushed toward the nearest wall, which was that of the inner pipes rather than the measurement wall. An interesting point to take into account when analyzing the experimental BSDs obtained, is the polydispersity of the bubble size distributions. According to the literature, the change in lift force direction occurs at a bubble diameter of 5.8 mm for the air–water system at ambient conditions. This behavior is of fundamental importance when performing CFD simulations of bubble columns,

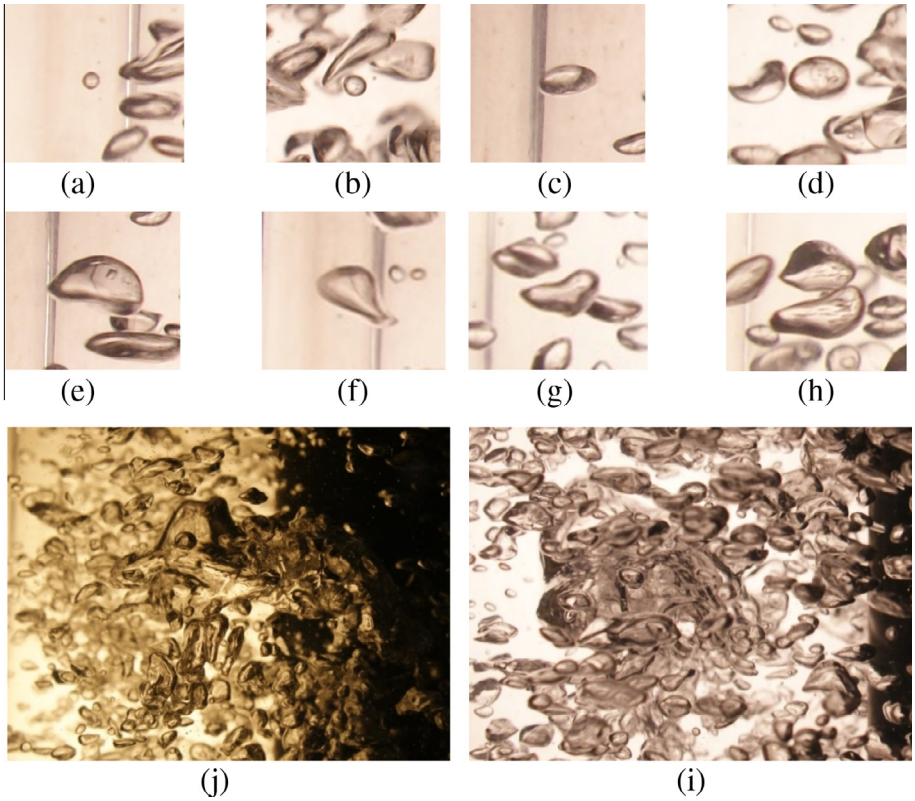

Fig. 7. Bubble shapes – U_G = 0.0087 m/s.

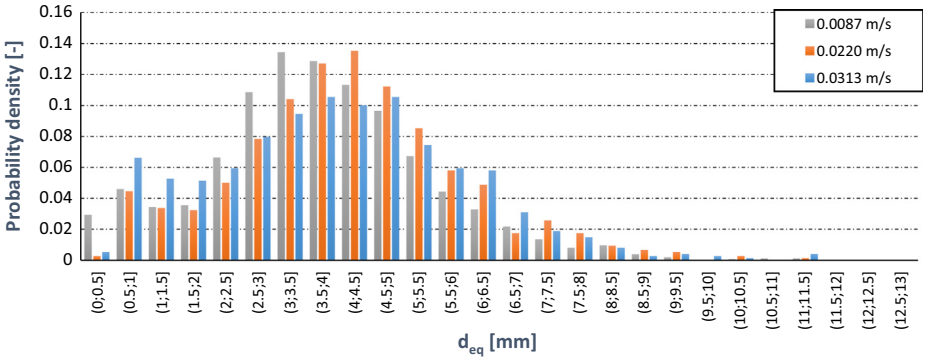

(a) Bubble size distribution

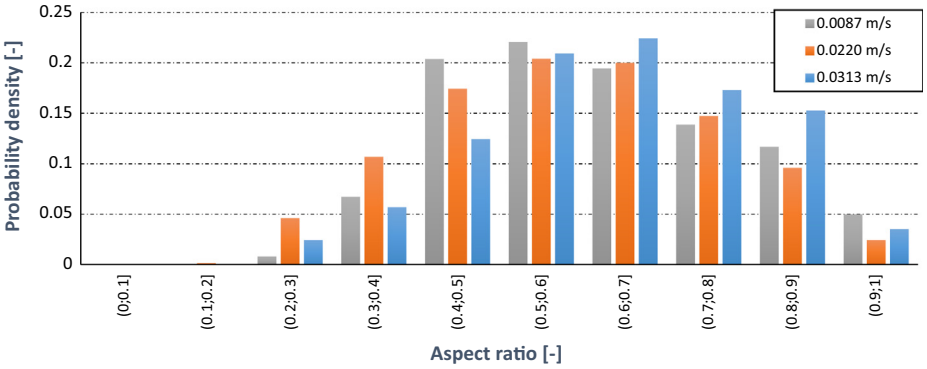

(b) Bubble aspect ratio distribution

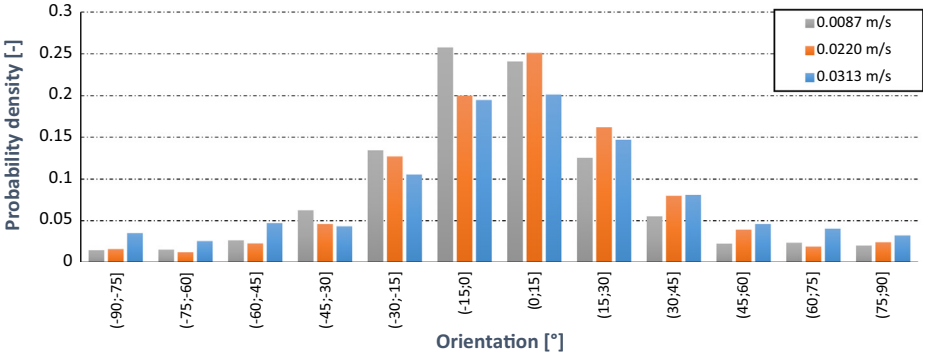

(c) Bubble orientation distribution

Fig. 8. Bubble diameter, aspect ratio and orientation distributions: influence of the superficial gas velocity – U_L = 0 m/s.

as discussed by different authors and should be taken into account if performing future numerical studies concerning this system [7,46,66].

Comparing the distributions of the equivalent diameters of the bubbles detected in the four areas (focusing the attention to U_G = 0.0087 m/s), it was observed that all four distributions were bimodal (Fig. 10a). The diameter distributions in areas 1, 3 and 4 had the absolute maximum frequency for equivalent diameters between 3 and 3.5 mm, whereas the relative maximum was between 0.5 and 1 mm. The distribution in area 2 featured the two maxima for diameters between 3.5 and 4 mm and a relative maximum between 1 and 1.5 mm. An interesting difference between the distributions is that, in area 1, there were more small bubbles than large ones. This means that near the wall, there were more small bubbles than large ones with respect to the internal area in the column. This may have been because of the lift force, which pushed the small bubbles toward the wall. The distributions of the equivalent diameters of bubbles detected in zones 3 and 4 can slightly deviate from the distributions of the bubbles present in those areas because of the passage of the cap-bubbles.

Lau et al. [67] conducted a study on the break-up phenomena in the bubbly flow regime in which the break-up of bubbles in terms of the critical Weber number We_{cr} was described. The authors reported two expressions for the calculation of We_{cr} for turbulent flows in pipes that can be used in this work for evaluating bubble stability (Table 4). For the sake of clearness, we just focus on U_G = 0.0087 m/s. The speed of the bubbles U necessary for the calculation of We was obtained by means of a graphical correlation (refer to the Section 3.2.6). The result was that the bubble samples were in the range of stability and not subject to breakage. The bubbles not sampled (i.e., the large cap-bubbles) were characterized by a greater Weber number than the critical one and could break into smaller bubbles. The same applied to the large bubbles, which were not detected because their irregular shapes were not approximated to oblate spheroids.

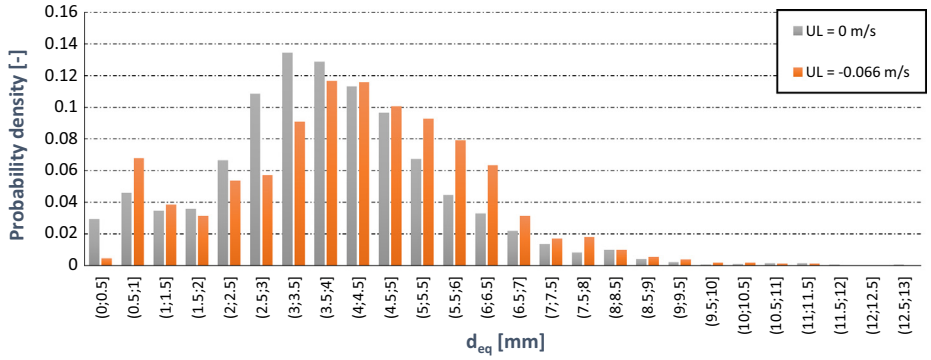

(a) Bubble size distribution

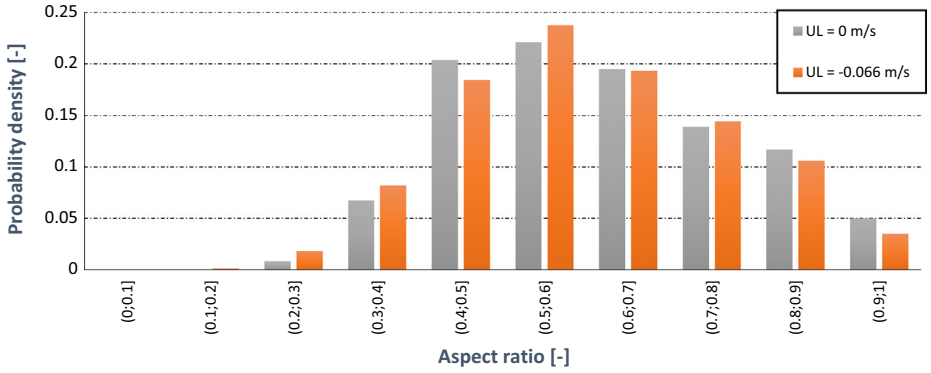

(b) Bubble aspect ratio distribution

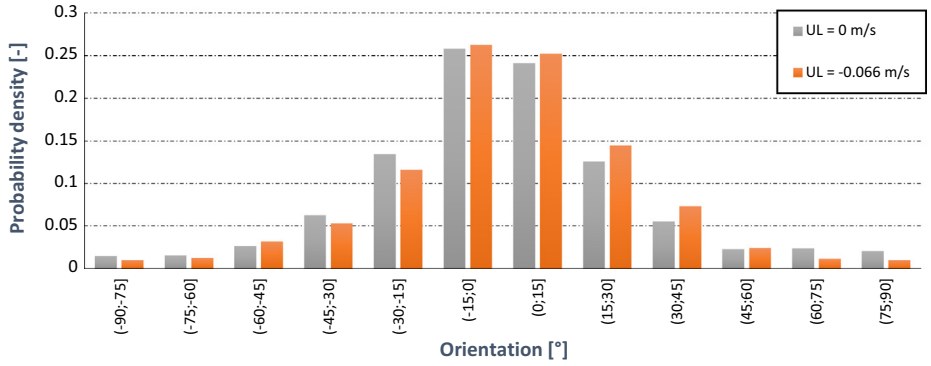

(c) Bubble orientation distribution

Fig. 9. Bubble diameter, aspect ratio and orientation distributions: influence of the superficial liquid velocity – $U_G = 0.0087$ m/s.

3.2.3. Bubble shape

Figs. 8b and 9b show the distribution of the aspect ratio of the bubbles for different superficial gas and water velocities, respectively. At $U_G = 0.0087$ m/s, five percent of the bubbles can be approximated as a sphere with φ between 0.9 and 1, 87% of the bubbles have $0.4 \leqslant \varphi \leqslant 0.9$ with a peak between 0.5% and 0.6%, and 6.7% are stretched along the major axis with $0.3 \leqslant \varphi \leqslant 0.4$; the remaining number of high distorted bubbles is negligible. Considering $U_G = 0.0202$ m/s we may notice some changes in the aspect ratio distribution: 2% of the bubbles have φ between 0.9% and 1.82% of the bubbles have $0.4 \leqslant \varphi \leqslant 0.9$, 11% have $0.3 \leqslant \varphi \leqslant 0.4$ and the remaining 5% have a lower aspect ratio. After the flow regime transition, at $U_G = 0.0313$ m/s, 4% of the bubbles have with φ between 0.9% and 1.88% of the bubbles have $0.4 \leqslant \varphi \leqslant 0.9$, 6% have $0.3 \leqslant \varphi \leqslant 0.4$ and the remaining 2% have $0 < \varphi \leqslant 0.3$. These results suggest that, as expected, when approaching the flow regime transition, large and distorted bubbles start appearing. Finally, increasing the water flow rate, expect for a slightly increase in the distorted bubbles, there are only small changes in the aspect ratio distribution: three percent of the bubbles have φ between $0.9 \leqslant \varphi \leqslant 1$, 86% of the bubbles have $0.4 \leqslant \varphi \leqslant 0.9$, 10% of the bubbles have $0.3 \leqslant \varphi \leqslant 0.4$ and the remaining 2% bubbles are highly distorted ($0 < \varphi \leqslant 0.3$).

Focusing our attention to $U_G = 0.0087$ m/s, there are no major discrepancies when considering the bubbles sampled in the different zones (Fig. 10b), confirming the nature of the dispersed flow. Instead, Fig. 11 ($U_G = 0.0037$ m/s) shows the centers of the bubbles; sizes are proportional to equivalent diameters, and colors correspond to aspect ratio. Near the wall, there are fewer large bubbles—as noted previously—but no general relation seems to exist between the aspect ratio and the position of the bubbles. Indeed, bubbles are uniformly distributed over the cross-section. However, a relationship between the size of the bubbles and the aspect ratio seems to exist. Indeed, analyzing the data in the d_{eq} – φ space (Fig. 12), we have found that the small bubbles have a high aspect ratio, whereas the larger bubbles seem to be characterized by

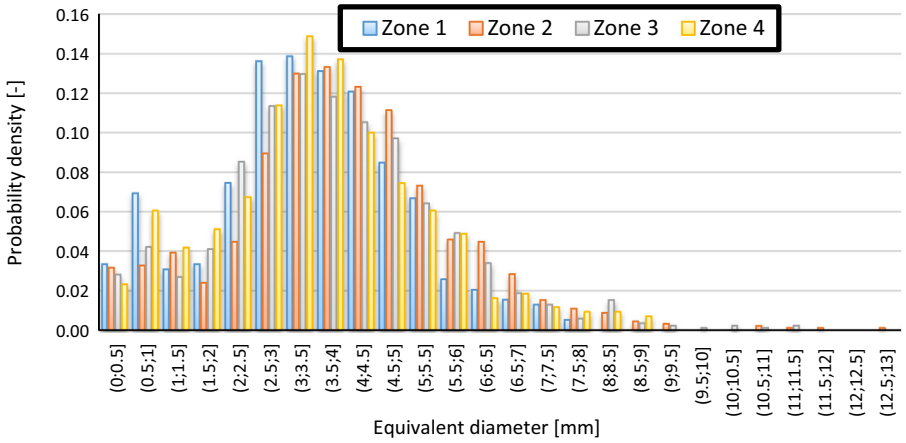

(a) Bubble size distribution

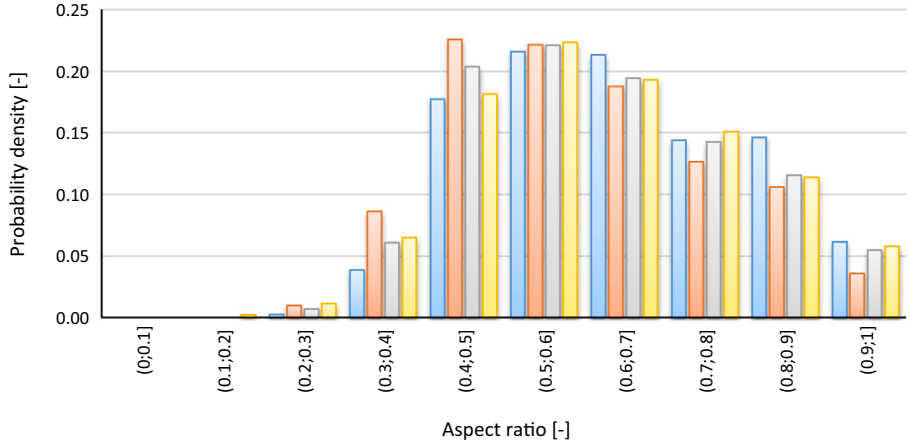

(b) Bubble aspect ratio distribution

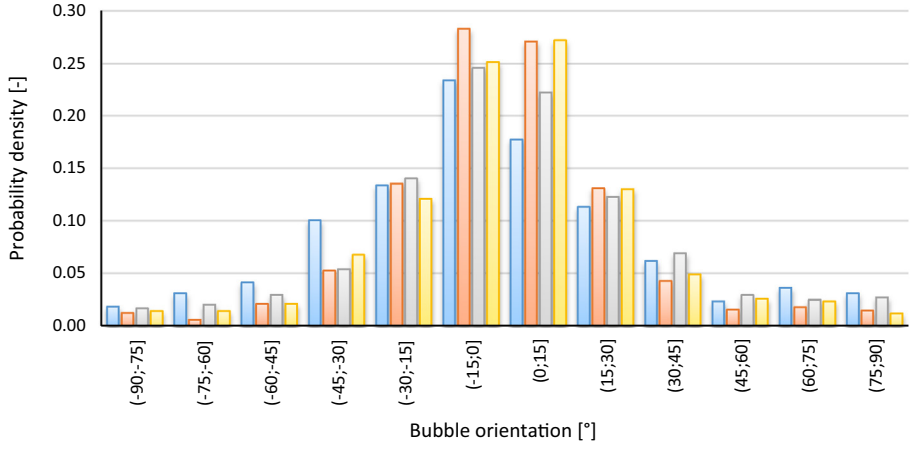

(c) Bubble orientation distribution

Fig. 10. Bubble diameter, aspect ratio and orientation distributions in the different zones – U_G = 0.0087 m/s and U_L = 0 m/s.

Table 4
Critical Weber number.

Reference	We_{cr} formulation	We_{cr} value	Equivalent stable diameter
Walter and Blanch [88]	$5,9\left(\frac{\mu_L}{\mu_G}\right)^{1/6}$	11.7	>12.8 mm
Hesketh, Fraser Russell and Etchells [89]	$1,1\left(\frac{\rho_L}{\rho_G}\right)^{1/3}$	9.9	>10.1 mm

lower aspect ratios. Indeed, bubbles with equivalent diameters less than 1 mm have an aspect ratio greater than 0.7. This means that the small bubbles tend to be spherical. Bubbles with higher equivalent diameters are characterized by lower aspect ratios (between 0.4 and 0.7), which reveals the trend of larger bubbles to be flatter. Between the different superficial gas velocities (Fig. 12a, c and d), the data in the d_{eq} – φ cover also the same area, but at U_G = 0.0313 m/s (Fig. 12d) there is an increase for the high d_{eq}

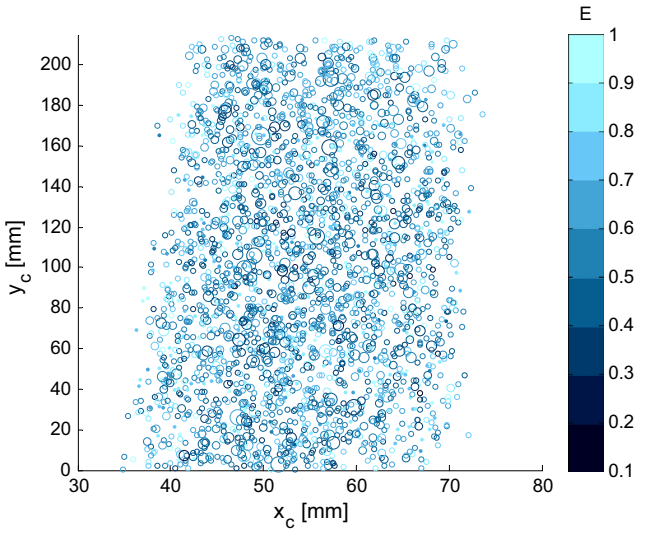

Fig. 11. Relation between the bubble position and the bubble shape and size – $U_G = 0.0087$ m/s.

bubbles. When considering the influence of the water velocity, we have not found any remarkable difference in the $d_{eq} - \varphi$ space (Fig. 12b).

3.2.4. Aspect ratio correlation

Several attempts have been made in the literature to correlate aspect ratio φ as a function of a dimensionless parameters. Some authors have used the Eötvös number *Eo* [68,69], others have adopted the Weber number *We* [69–71], and Tadaki and Maeda [72] used a dimensionless group defined as a function of the Reynolds and Morton numbers that was later named the Tadaki number [73]. Others have used more than one dimensional number—e.g., Bozzano and Dente used both *Mo* and *Eo* [74]. These correlations are obtained for single rising bubbles and are frequently applied in methods to relate chord length distributions to BSDs [75]. A large number of studies have focused on rising bubbles, and these correlations have been compared in a large dataset by Celata et al. [76–78]. However, when considering bubbly flows, these correlations may not be suitable.

The goal of this section is to assess a simple correlation between non-dimensional parameters and the aspect ratio for bubbly flow and compare it to the results of previous literature. The experimental data obtained are used, and the procedure applied by Wellet et al. [69] is considered as a reference.

At first, we consider the dataset obtained for $U_G = 0.0087$ m/s. The aspect ratio data (Fig. 12a) are scattered broadly; therefore, the data are grouped into classes of equivalent diameters. Each class is represented by the average aspect ratio of the bubbles belonging to that class. Because 99.5% of the bubbles are included within the class of $d_{eq} = 8.87$ mm, bubbles with higher equivalent diameters are not considered. The relationship between the deformation of the bubbles—described by aspect ratio φ—as well as the size of the bubbles, speed of the bubbles and physical properties of the system may be written as a function of the following parameters:

$$\varphi = f(v, \sigma, d_{eq}, \mu_L, \mu_G, \rho_L, \Delta\rho, g) \tag{17}$$

By means of the dimensional analysis:

$$\varphi = f\left(\frac{d_{eq} v^2 \rho_L}{\sigma}, \frac{d_{eq} v \rho_L}{\mu_L}, \frac{g\Delta\rho d_{eq}^2}{\sigma}, \frac{v^2}{g d_{eq}}, \frac{\mu_L}{\mu_G}\right) = f(We, Re, Eo, Fr, N_{\mu_r}) \tag{18}$$

A different formulation can be used for f, and—in this paper—the same expression proposed by Wellek et al. [69] is used:

$$\frac{1}{\varphi} - 1 = \alpha_0 \cdot (We)^{\alpha_1} \cdot (Re)^{\alpha_2} \cdot (Eo)^{\alpha_3} \cdot (Fr)^{\alpha_4} \cdot (N_{\mu_r})^{\alpha_5} \tag{19}$$

The coefficients α_0, α_1, α_2, α_3, α_4 and α_5 are evaluated by using a multiple regression program that progressively adds independent variables, starting from the most important and ending with the dimensionless groups statistically less significant for the correlation. As a result, it was noticed that the use of multiple dimensionless numbers did not provide a benefit, and a single non-dimensional parameter can approximate the present system. This is in accordance with the results of Wellek et al., and the following relation is used:

$$\frac{1}{\varphi} - 1 = \alpha_0 \cdot (Eo)^{\alpha_3} \tag{20}$$

Hence, the aspect ratio reads:

$$\varphi = \frac{1}{1 + \alpha_0 \cdot (Eo)^{\alpha_3}} \tag{21}$$

By using the least squares estimation to evaluate the coefficients, the results are $\alpha_0 = 0536$ and $\alpha_3 = 0292$; the confidence intervals at 95% of the coefficients are 0.536 ± 0.027 and 0.292 ± 0.032, respectively:

$$\varphi = \frac{1}{1 + 0.536 \cdot (Eo)^{0.292}} \tag{22}$$

This correlation is similar to the correlations developed by Wellek et al. [69] and Okawa et al. [68]. The correlation of Wellek et al. [69] was originally developed for non-oscillating drops in contaminated liquids, and—according to Fan and Tsuchiya [79]—it appears to be extendible even to oscillating bubbles in low-viscosity liquids:

$$\frac{1}{\varphi} = \frac{1}{1 + 0.163 \cdot (Eo)^{0.757}} \tag{23}$$

Okawa et al. modified the above correlation to fit the lower boundary of their data:

$$\frac{1}{\varphi} = \frac{1}{1 + 1.97 \cdot (Eo)^{1.3}} \tag{24}$$

The comparison among Eqs. (23), (24), the present correlation (Eq. (22)) and the experimental data is shown in Fig. 13a, in which φ is plotted against *Eo*. The Wellek correlation overestimates the aspect ratio, the Okawa correlation is unable to correlate the aspect ratio, and the developed correlation fits the data fairly well. The average of the absolute deviations of the experimental data from the developed correlation is equal to 3.2%. This suggests that correlations taken from the literature should be carefully evaluated before being applied to dense bubbly flows. It is worth noting that—owing to the point selection for ellipse fitting—the smaller the bubble, the larger the error of estimation (Appendix B). This should in principal change the results in Fig. 13a, thus causing the line to fit better with the correlation of Wellek et al.

The correlation obtained (Eq. (22)) was derived considering only the data for $U_G = 0.0087$ m/s. However, the validity of this correlation should be verified considering other operating conditions. For this reason, now, we consider all the experimental data obtained. Following the same procedure described above, the resulting coefficients of the correlation are the following: $\alpha_0 = 0553$ and $\alpha_3 = 0.266$; the confidence intervals at 95% of the coefficients are 0.553 ± 0.028 and 0.266 ± 0.034, respectively. The resulting correlation is:

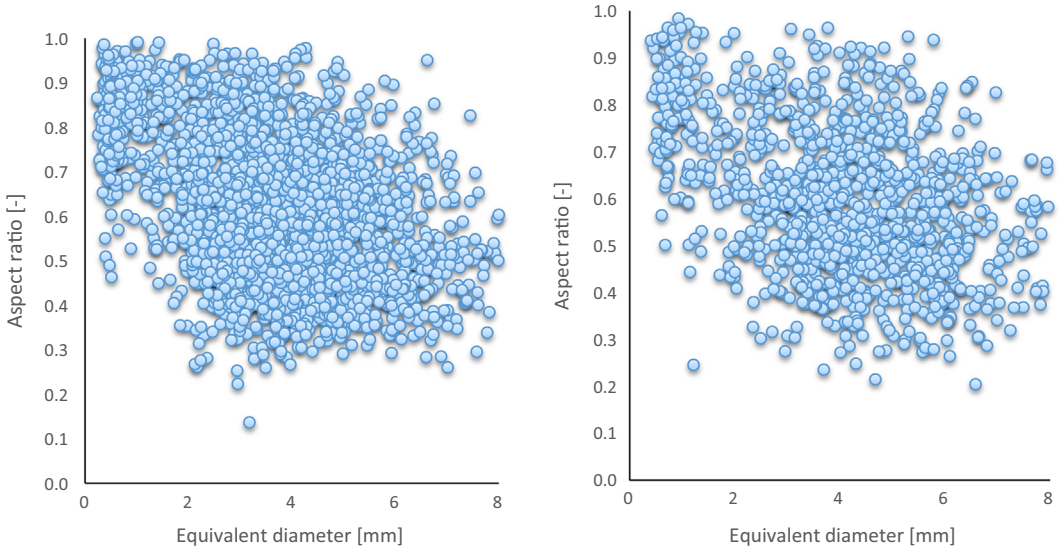

(a) U_G = 0.0087 m/s – U_L = 0 m/s

(b) U_G = 0. 0087 m/s – U_L = - 0.04 m/s

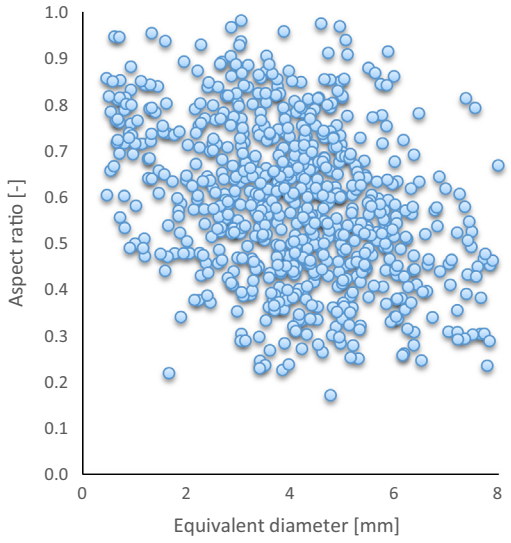

(c) U_G = 0.0220 m/s – U_L = 0 m/s

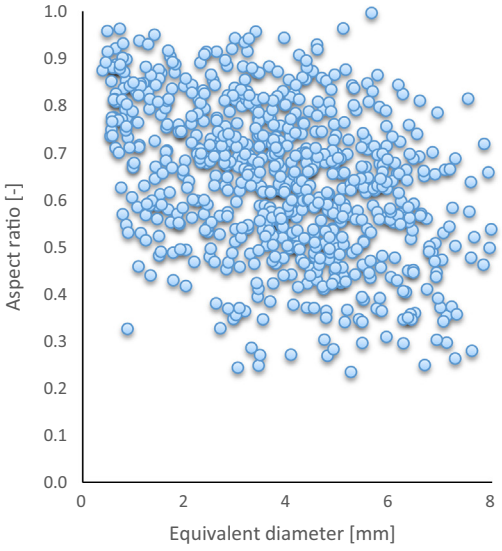

(d) U_G = 0.0313 m/s – U_L = 0 m/s

Fig. 12. Bubble aspect ratio distributions.

$$\varphi = \frac{1}{1 + 0.553 \cdot (Eo)^{0.266}} \tag{25}$$

The comparison between Eqs. (22) and (25), as well as the two different datasets, may be found in Fig. 13b. There are not major differences between the two correlations and datasets: this suggests that the bubble shape and size distribution does not depend on the operating condition as long as the geometrical configuration is the same and a large dataset is considered.

3.2.5. Bubble orientation

Figs. 8c and 9c show the distribution of the bubble orientation for different superficial gas and water velocities, respectively. There are no remarkable difference between the different cases. Generally speaking, fifty percent of the bubbles have an orientation between −15° and +15°, and 75% have an orientation between −30° and +30°. The distributions of the bubble orientations in the four zones have no remarkable differences, confirming the nature of the dispersed flow (Fig. 10c). This distribution of the angles around the value 0 may indicate that the bubbles move predominantly upward in a zigzag motion with angles ranging from −30° to 30°.

3.2.6. Comparison with the literature

In the literature, experimental studies concerning swarms of rising bubbles and the bubbly flow in annular gap bubble columns are limited. Therefore, studies concerning rising bubbles are considered as references for comparing the bubble shapes. In this section, the data obtained at U_G = 0.0087 m/s are considered, but the results may be generalized for all the others conditions studied, without the loss of generality.

For bubbles rising in an infinite medium, Clift et al. [73] proposed a graphical correlation to determine the shape of the bubbles in terms of *Eo*, *M* and *Re*. *M* is defined only by the properties of the fluids, and for a constant *M*, the shapes of the bubbles evolve from spherical to ellipsoidal to cap-shaped with increasing

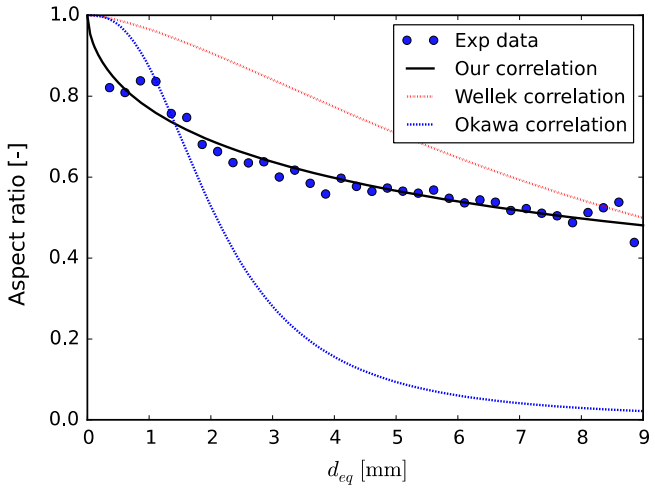

(a) *Correlation comparison (U_G = 0.0087 m/s)*

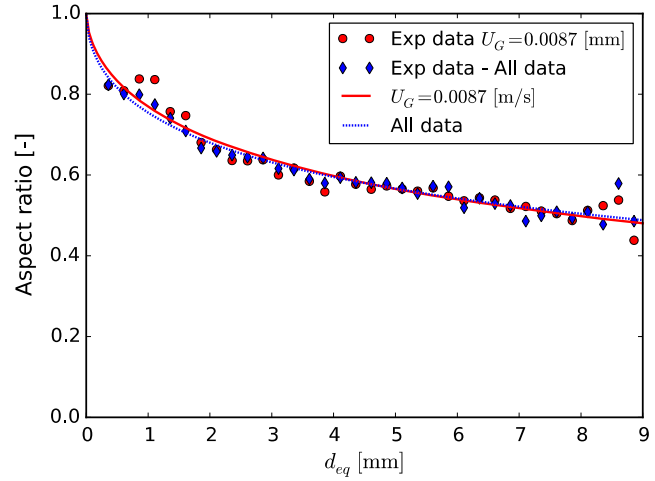

(b) *Comparison between the correlation obtained with U_G = 0.0087 m/s and using the whole dataset*

Fig. 13. Aspect ratio correlation.

equivalent diameter. Clift et al. evaluated influence of the wall on the rising bubbles according to the ratio λ between the equivalent diameter of the bubble and the diameter of the system. For values of λ less than 0.6, the walls have little influence, and the rising bubble can be considered as if rising in an infinite medium. The largest bubble detected in this analysis had an equivalent diameter of 12.6 mm, and the hydraulic diameter of the column with an internal pipe is equal to 129 mm. The maximum value of λ is therefore 0.1. Thus, the effect of the wall can be neglected as a first approximation. This diagram can be used to derive the terminal velocity v for each bubble: knowing *Eo* and *M*, *Re* can be derived and, thus, so can the equivalent bubble terminal velocity v. This is, of course, an approximation because this diagram has been obtained for single rising bubbles rather than swarms of rising bubbles. The velocity obtained is not the real bubble velocity but is the equivalent velocity of the bubble in the present system if placed in an infinite medium. The data are represented in Fig. 14 as a function of the aspect ratio. The Reynolds number and terminal velocity of the bubbles increase with the equivalent diameter of the bubbles and have ranges of 8–3102 and 0.03–0.27 m/s, respectively. With regard to the shapes of the bubbles, the data obtained from the analysis of the images are in agreement with the diagram by Clift et al. Bubbles with aspect ratio near 1 are placed in the area of spherical bubbles; in the ellipsoidal area, the bubbles possess a higher aspect ratio. There is no bubble in the area of the cap-bubbles; indeed, cap-bubbles were not detected.

Cano-Lozano et al. [80] used the Bond and the Galilei number to describe the shape of the bubbles. They represented the bubbles in space *Bo–Ga*, coloring them according to the value of the inverse aspect ratio. Fig. 15 shows the experimental data in *Bo–Ga* space, revealing good agreement with the literature.

4. Image analysis for supporting flow regime transition prediction: the stability analysis

In this section, we use the image analysis as a supporting tool for the evaluation of the flow regime transition in the framework of the stability analysis.

4.1. Stability analysis: methods description

We employ the approach of Bhole and Joshi [29] based on the one-dimensional model of gas–liquid dispersion in Euler–Euler framework. In this section the derivation of the criteria is outlined for the sake of completeness, but the detailed mathematical formulation will not be repeated, because detailed elsewhere [29]:

i. The balance equations (continuity and moment) are written for the gas liquid system.
ii. The momentum equations of both the phases are combined by eliminating the pressure term.
iii. Perturbations are introduced in the balance equations in terms of perturbation variables.
iv. The resulting equations are linearized.
v. The velocity perturbations are eliminated using the equations of continuity, and a final linearized equation is obtained in terms of perturbation in holdup.

In the homogeneous regime, any perturbation to the flat holdup profile decays with respect to time. If the perturbations grow with time, the transition to the heterogeneous regime occurs. The stability criterion is given by the following equation:

$$f = 1 - \frac{\left[A\left(\frac{G}{F}\right) - \frac{B}{2}\right]^2}{A(Z - C) + \frac{B^2}{4}} \tag{26}$$

The system is stable if f is positive, unstable if f is negative and neutrally stable when $f = 0$. The constants A, B, C, Z, F and G are given by:

$$A = \frac{\rho_G}{\rho_L} + \frac{(1 + C_V)}{(1 - \varepsilon_G)} - 1 \tag{27}$$

$$B = 2\left[\frac{\rho_G}{\rho_L} + C_V\right]\frac{U_G}{\varepsilon_G} \tag{28}$$

$$C = \left[\frac{\rho_G}{\rho_L} + C_V\right]\left(\frac{U_G}{\varepsilon_G}\right)^2 \tag{29}$$

$$Z = -\frac{\beta_0}{\rho_L}\left[\frac{D_L}{\varepsilon_G} + \frac{D_G}{1 - \varepsilon_G}\right] \tag{30}$$

$$F = \frac{\beta_0}{\rho_L}\left[\frac{1}{\varepsilon_G} + \frac{1}{1 - \varepsilon_G}\right] \tag{31}$$

$$G = \frac{\beta_0}{\rho_L}\frac{V_S}{\varepsilon_G} + V_S\frac{\beta_0'}{\rho_L} + \frac{\rho_G - \rho_L}{\rho_L}g \tag{32}$$

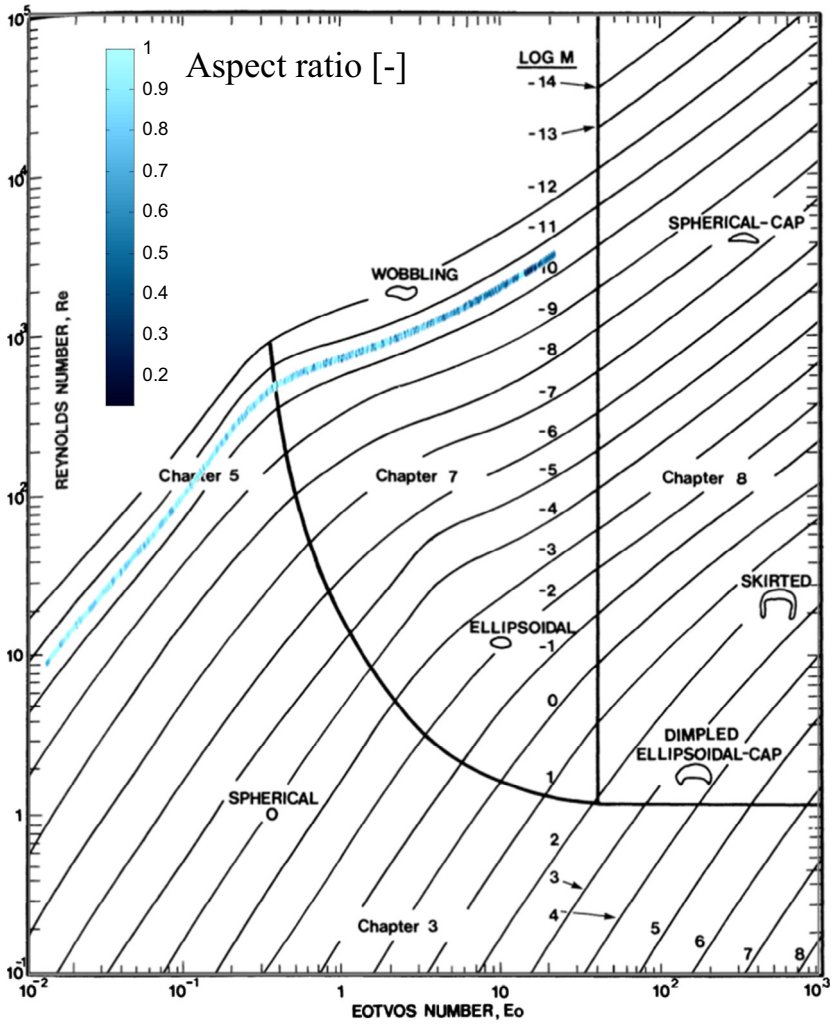

Fig. 14. Comparison with non-dimensional diagrams: Clift diagram.

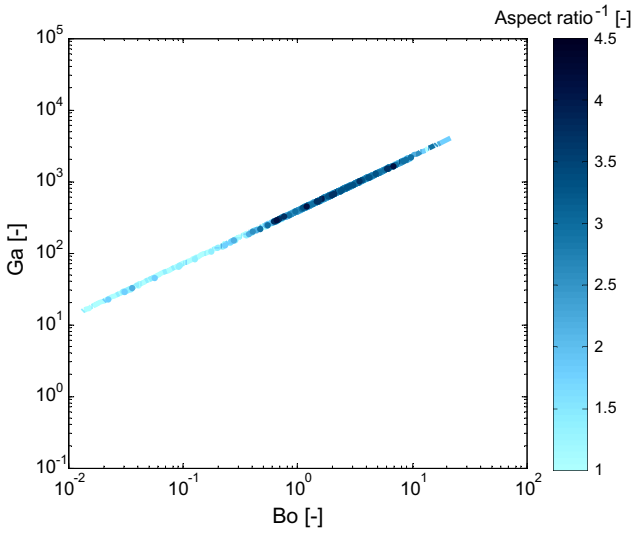

Fig. 15. Comparison with non-dimensional diagrams: Bo–Ga diagram.

where

$$\beta_0 = \frac{\varepsilon_G(\rho_G - \rho_L)}{V_S} g \tag{33}$$

$$\beta_0' = -\frac{\varepsilon_G(\rho_G - \rho_L)}{V_S} g \tag{34}$$

Using the above values of constants, the critical gas holdup at which homogeneous regime loses stability, can be obtained by the following implicit equation:

$$\frac{u_\infty}{\sqrt{g d_b}} = \left[\sqrt{\frac{\vartheta(1-\varepsilon_G)}{C_{V0}(1+2\varepsilon_G)+(1-\varepsilon_G)^2}}\right] \frac{1}{(1-\varepsilon_G)^{m-1}} \tag{35}$$

The reader should refer to the original reference for further details and for all the mathematical formulations of the method.

4.2. Stability analysis: model parameters

To use the stability criterion for the quantitative predictions of the transition in bubble columns, various parameters need to be estimated.

4.2.1. Slip velocity

Slip velocity V_S is estimated using Richardson–Zaki correlation, previously reported in Eq. (12):

$$V_S = U_b = u_\infty (1-\varepsilon_G)^{n-1} \tag{36}$$

The same considerations applied before, are also valid here.

4.2.2. Dispersion coefficient

The gas-phase dispersion coefficient can be written as the product of integral velocity and length scales of the turbulence:

$$D_G = u'l \tag{37}$$

Joshi [81] has used energy balance for the estimation of u', where the length scale of the turbulence in the bubbly flow is assumed to be twice the bubble diameter:

$$u' = 1.5\varepsilon_G \tag{38}$$

$$l = 2b_b \tag{39}$$

Bhole and Joshi [29] use the constant of proportionality 3 as a preliminary estimate:

$$D_G = 3\varepsilon_G d_b \tag{40}$$

In this paper, we employ the same coefficient as in the original reference and sensitivity analysis have been performed (Section 4.4). Accordingly with the original reference, d_b is evaluated accordingly with the correlation proposed by Nguyen [82], instead of the experimental data:

$$d_b = u_\infty \frac{3}{4} \tag{41}$$

4.2.3. Virtual mass coefficient and the importance of the image analysis

As the bubble accelerates through the liquid, a certain mass of the liquid surrounding the bubble also needs to be accelerated [83]. The mass associated with the liquid to be accelerated is referred to as virtual mass of the bubble and the additional force thus required is referred to as added mass force. From the application of potential flow theory results that $C_v = 0.5$ for an isolated spherical bubble in an infinite inviscid liquid. The dependence of added mass coefficient on the gas holdup has been shown by Zuber [84]:

$$C_v = \frac{1}{2}\left(\frac{1+2\varepsilon_G}{1-\varepsilon_G}\right) \tag{42}$$

In Eq. (42) $C_v = 0.5$, when ε_G tends to 0 and, in the following, we refer to this value as C_{v0}. However, this result is valid for a spherical bubble only and, in bubble columns, the bubbles are likely to be oblate ellipsoidal. The value of C_{v0} depends upon the extent of deformation of spherical bubble. Bhole and Joshi [29] generalized the $C_v - \varepsilon_G$ relationship suggested by Zuber:

$$C_v = C_{v0}\left(\frac{1+2\varepsilon_G}{1-\varepsilon_G}\right) \tag{43}$$

C_{v0} can be estimated knowing the bubble aspect ratio ϕ. For oblate oblate ellipsoidal bubbles Clift et al. [73] have obtained the following relation:

$$C_{v0} = \frac{\varphi\cos^{-1}\varphi - (1-\varphi^2)^{0.5}}{\varphi^2(1-\varphi^2)^{0.5} - \varphi\cos^{-1}\varphi} \tag{44}$$

The critical issue is to relate the aspect ratio φ to parameters depending on the system. As previously presented in Section 3.2.4, the correlation available in the literature for single bubbles may not be suitable for bubbly flows and the correlation obtained din this study (Eq. (22)) is here used. Sensitivity analysis concerning the correlation used are proposed in the results discussion (Section 4.4).

Table 5
Flow regime transition: experimental data, stability analysis and literature correlations.

	Exp.	Stability analysis	Wilkinson et al. [86]	Reilly et al. [85]
U_{trans} (m/s)	0.0263	0.0266	0.00198	0.0289
$\varepsilon_{G,trans}$ (−)	0.0874	0.1100	0.0077	0.1295

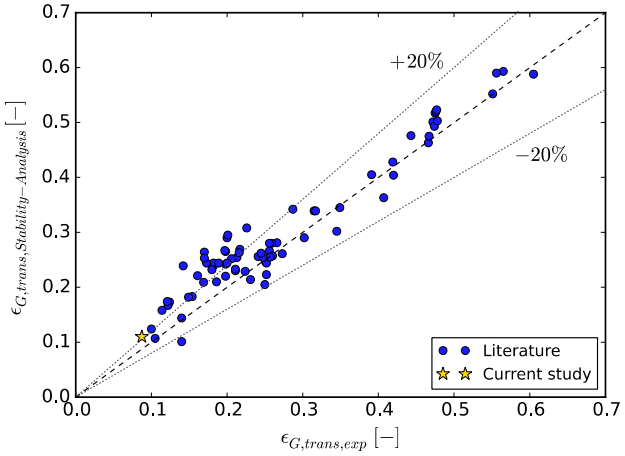

Fig. 16. Stability analysis: comparison between present result and the literature.

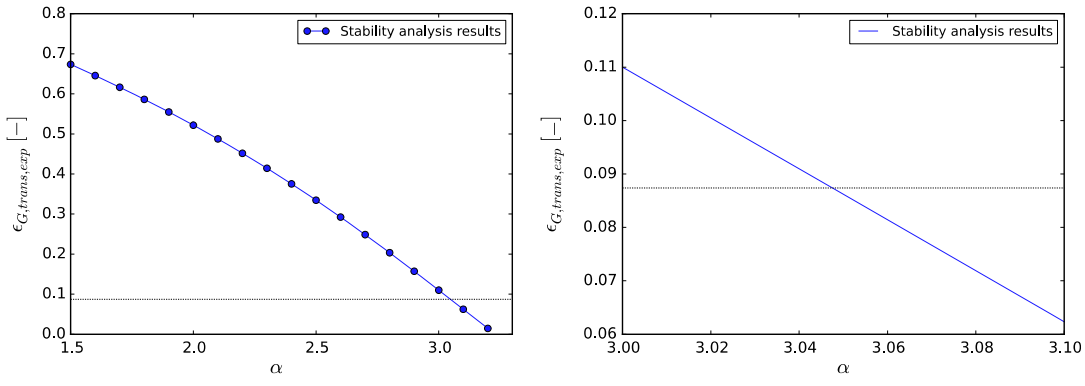

(a) Holdup **(b) Swarm velocity**

Fig. 17. Stability analysis: influence of the dispersion coefficient on the transitional holdup.

4.3. Evaluation of the transitional velocity

The stability analysis method provides the value for the transitional holdup. In order to have an estimate of the transitional velocity, the above criteria could be coupled with a correlation form the literature. The correlation is from Reilly et al. [85] is taken:

$$U_{trans} = \frac{\rho_L}{\rho_G}(1 - \varepsilon_{G.trans})\left(\frac{B^*}{A^*}\right)^{1.5} \tag{45}$$

In the original reference the transitional holdup reads:

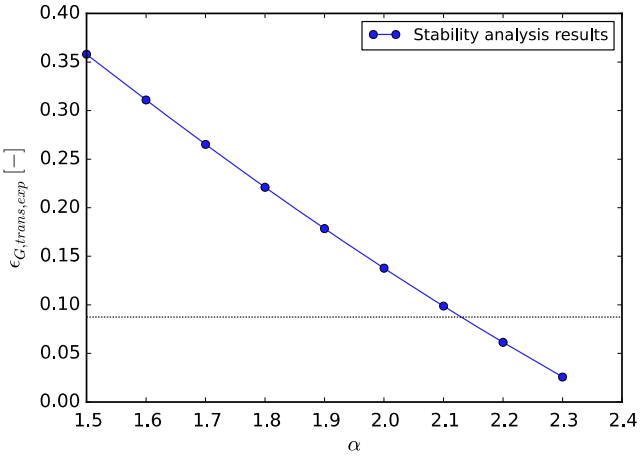

Fig. 18. Stability analysis using the Wellek correlation for the aspect ratio.

$$\varepsilon_{G.trans} = 0.59B^{*1.5}\left(\frac{\sigma^{0.12}\rho_G^{0.96}}{\rho_L}\right)^{0.5} \tag{46}$$

In this paper, the holdup at the transition provided by Eq. (35). Finally, A^* reads:

$$A^* = 2.81\rho_L\rho_G^{0.96}\sigma^{-0.12} \tag{47}$$

For water as the liquid phase, $B^* = 3.75$.

4.4. Stability analysis: the results

Applying the Eq. (35) and using the virtual mass formulation with our correlation for the aspect ratio, Eq. (22), the transitions holdup is 0.11 (Table 5), showing a good agreement with the experimental data. This result is also in agreements with the capability of the linear stability analysis for the prediction of the transition point in bubble columns. The summary of the previous results of the linear stability are given in Fig. 16 (the data have been obtained from Ghatege et al. [34]). It is particularly interesting that, applying Eq. (45) along with the results of the stability analysis, the resulting transitional velocity ($U_{trans,stability\ analysis} = 0.0266$ m/s) is in perfect agreement with the experimental data ($U_{trans} = 0.0263$ m/s). This support the idea of coupling the Reilly correlation to the stability method. However, a comprehensive validation of this approach should be performed on a larger set of experimental data.

The obtained results are also compared with literature correlations: Wilkinson et al. [86] and Reilly et al. [85]. The Wilkinson correlation largely underestimates the transition gas velocity; this observation was also made by Letzel et al. [87] and is a well-known result from the literature: this correlation usually under predict the transition velocity and holdup at the atmospheric

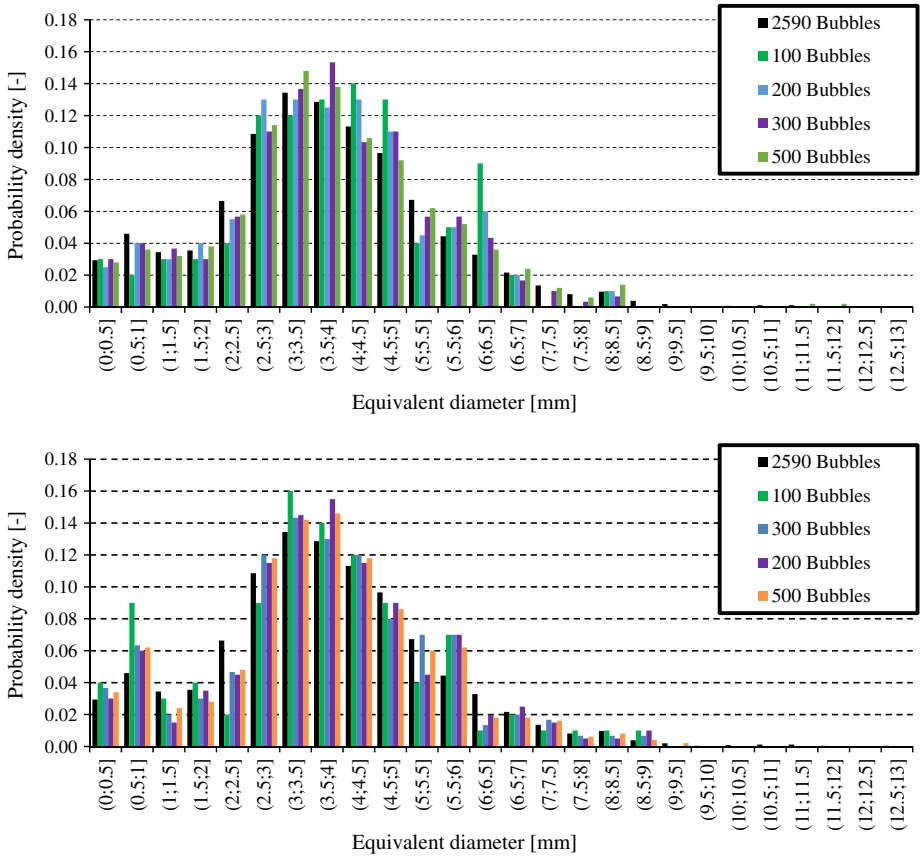

Fig. 19. BSDs as a function of the number of bubbles sampled: two samplings of random bubble.

conditions. The Reilly correlation, instead, gives values for U_{trans} and $\varepsilon_{G,trans}$ that are in better agreement with the experimental data. However, the stability method (coupled with the Reilly correlation) is able to provide better results if compared with the other correlations. The stability analysis, therefore, is an accurate tool for the prediction of the transition point also for annular gap configuration. To the author's best knowledge, the only previous results for the stability analysis for an annular gap configuration was proposed by Bhole et al. [33] with the data of al-Oufi et al. [57].

Bhole and Joshi [29] discussed about the dispersion coefficient. In this study, the value of the proportionality constant for dispersion appearing in Eq. (40) was set to 3 as a preliminary estimate ($\alpha = 3$), following the original reference. This value proved to be adequate for predicting the transition point (Table 5). However, it is useful to vary this parameter. Fig. 17a shows the variation of transition gas holdup with α as a parameter. The results are in agreements with the original reference: as the value of α increases, the transition gas holdup also increases. Indeed, an increase in α indicates an increase in the dispersion coefficient, which stabilizes the systems. The mechanism of dispersion tries to counterbalance the effect of non-uniformity in the holdup and hence it is responsible for the minimization of gradients in the system. Thus, higher the value of the dispersion coefficient (given by α), the higher is the value of the transition holdup. Of course, we may use this parameter in order to fit the experimental data. A dispersion coefficient of 3.05 (Fig. 17b) provide the transition velocity equal to the one of the experimental setup. The value is very close to 3, suggesting that the first guess taken from the literature was correct. This suggests that in future studies, a more detailed model for the dispersion coefficient should be employed. Eventually, a coefficient depending on the operating condition, working fluid and geometry should be applied.

Finally, the influence of the aspect ratio correlation has been investigated by applying the Wellek and the Okawa correlation. The results for the Wellek formulation are presented in the Fig. 18: the dispersion coefficient to be used, for having a correct

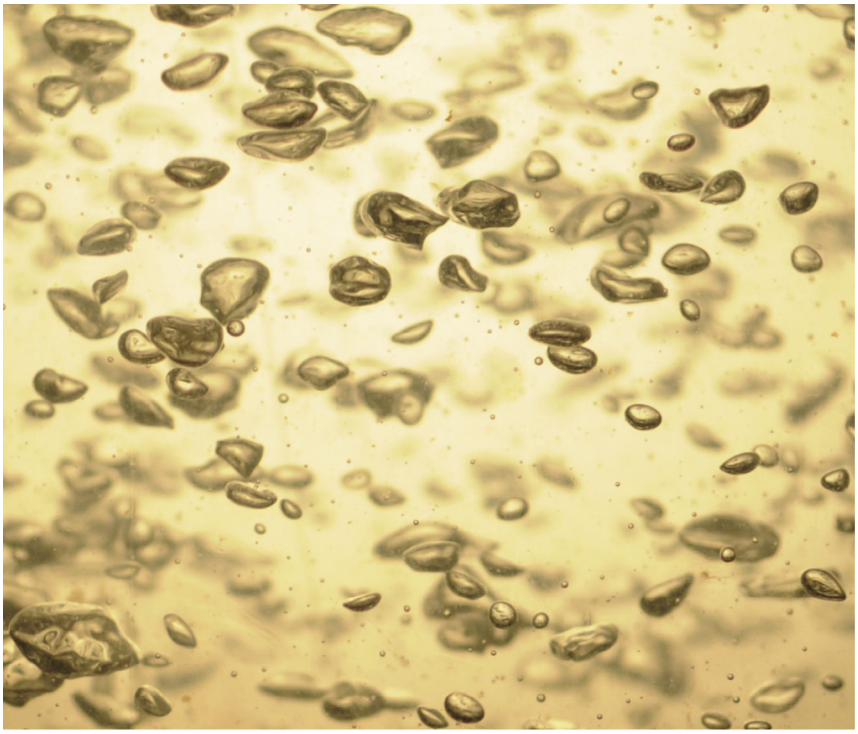

(a) Image selected

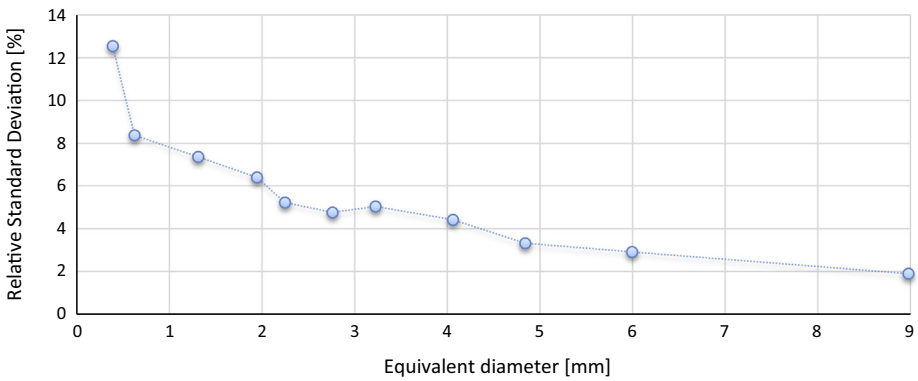

(b) Relative standard deviation as a function of the equivalent diameter

Fig. 20. Error analysis.

Table 6
Bubble classes in the error analysis.

Number of class	d_{eq} (mm)
1	$0 < d_{eq} \leqslant 0.5$
2	$0.5 < d_{eq} \leqslant 1$
3	$1 < d_{eq} \leqslant 1.5$
4	$1.5 < d_{eq} \leqslant 2$
5	$2 < d_{eq} \leqslant 2.5$
6	$2.5 < d_{eq} \leqslant 3.5$
7	$3.5 < d_{eq} \leqslant 4.5$
8	$4.5 < d_{eq} \leqslant 6$
9	$6 < d_{eq} \leqslant 8$
10	$8 < d_{eq} \leqslant 10$
11	$d_{eq} > 10$

value of the transitional holdup is around 2.1. This happen because the Wellek correlation predicts bubbles with higher aspect ratio and, therefore, the homogeneous flow regime can be destabilized more easily. When applying the Okawa correlation, instead, the result are non-physical. This is because the Okawa correlation greatly under predicts the experimental aspect ratio and, therefore, the flow is very difficult to be destabilized for the given bubble diameter (Eq. (24)).

5. Conclusions

An understanding of the properties, diameter distribution and shape of bubbles is of fundamental importance in the comprehension of the flow dynamics and mass transfer phenomena for the correct design and operation of bubble column. In the literature, a large number of studies have focused on open tube bubble column, but the knowledge concerning bubble column with internals is very limited. This paper considers an annular gap bubble with an inner diameter of 0.24 m with two internal pipes and is, mainly, structured in two parts.

The first part of the paper concerns the experimental investigation: holdup measurements and image analysis. The former is used for identifying the flow regime transition and studying the bubble column hydrodynamics, whereas the latter is used for investigating the bubble shapes and size distributions. The holdup measurements and the transition point and discussed and are in agreement with the previous literature concerning distributors with large openings. The definition of the transition point is important because the size distribution and bubble shapes depend on the operating conditions and a change of the bubble properties is expected near the transition. The image analysis is applied at different superficial gas and liquid velocities, corresponding to a gas holdup between 2.9% and 9.6%. In particular, the homogeneous flow regime (and the beginning of the transition flow regime) has been considered. In this flow regime, the bubbles are uniformly distributed in the cross-section of the pipe, traveling vertically with minor transverse and axial oscillations; however, there is also the periodic appearance of cap-bubbles around the inner pipes. These cap bubbles raise the column at a higher velocity compared to the other bubbles; they drag in their wake swarms of smaller bubbles and generate break-up phenomena in the path. Owing to the presence of the cap-bubbles, this regime can be better defined as a pseudo-homogeneous regime. The bubble size distributions and shapes are presented and discussed for different superficial gas and liquid velocities. The bubble diameter distributions are bimodal and a change in the bubble size is noticed near the flow regime transition. No general relation seems to exist between the aspect ratio and the position of the bubbles; however, a relationship between the size of the bubbles and the aspect ratio seems to exist: the small bubbles have a high aspect ratio, whereas the larger bubbles seem to be characterized by lower aspect ratios. This distribution of the angles around the value 0 may indicate that the bubbles move predominantly upward in a zigzag motion with angles ranging from $-30°$ to $30°$. The experimental data are also used to obtain a correlation between non-dimensional parameters and the aspect ratio. This correlation does not depen on the gas and liquid velocities and performs better compared to correlations from the literature. Finally, the experimental data were compared to non-dimensional diagrams taken from the literature, revealing a good correspondence.

The second part of the paper concerns the application of the image analysis results as supporting tool for the evaluation of the flow regime transition in the stability analysis framework. In the mathematical formulation of the stability analysis approach, the virtual mass coefficient appears and it depends on the bubble shape: the correlation obtained from the experimental data is used. The stability analysis provided the transitional point (holdup and gas velocity) in very good agreement with experimental data and the method performed better than the correlations from the literature. Finally, sensitivity analysis concerning the dispersion coefficient and the virtual mass formulation was performed, proving that the correct evaluation of these parameters is of fundamental importance in the formulation of the method.

The present experimental investigation may provide a better understanding of the two-phase flow phenomena in annular gap bubble columns. The analysis in this paper can provide useful information for the CFD modeling of annular gap bubble columns [7]: for example, an Eulerian–Eulerian approach can be considered. Such an approach requires information concerning BSD and bubble shapes, which have been presented in this work. Furthermore, the analysis of such low holdups can assist in understanding more complex flows and for scaling-up purposes. Finally, this paper extended the stability analysis to an annular gap bubble column, proving its ability in investigating the flow regime transition. This study details the major issue of the stability analysis approach and proposed methodology for dealing with the aspect ratio formulation and the dispersion coefficient. Future studies should focus on the modeling of the dispersion coefficient and find a general model for the virtual mass coefficient. This paper also demonstrates the application of different experimental techniques for a comprehensive knowledge of the bubble column hydrodynamic.

Acknowledgments

The authors would like to thank the anonymous reviewers for their valuable comments and suggestions to improve the quality of the paper. The authors thank Medea Carrara for the help in implementing the image analysis method and the image samplings. The authors also thank Francesca Besagni for the suggestions concerning the acquisition of the photos.

Appendix A

An analysis was performed on the number of bubbles to be sampled to achieve a reliable BSD. To perform this analysis, a random number was first assigned to each bubble, then the bubbles were sorted in ascending order and, finally, were sampled in groups of 100, 200, 300 and 500 bubbles. Fig. 19 presents two BSDs resulting from the generation of two random number sequences. It seems as if approximately 300 bubbles can provide a reliable BSD for the configuration studied.

Appendix B

An analysis was performed to evaluate the error in the bubble shape estimation due to the handpicked points. The analysis was conducted as follows:-

(a) An image was selected (Fig. 20a) and sampled 20 different times, thus obtaining a dataset comprising 540 bubbles;
(b) This dataset was divided into 11 classes of bubbles (Table 6);
(c) For each class, the mean value, standard deviation and standard deviation relative to the mean value was obtained (Fig. 20b).

As expected—owing to the point selection for ellipse fitting—the smaller the bubble, the larger the estimation error.

References

[1] N. Kantarci, F. Borak, K.O. Ulgen, Bubble column reactors, Process Biochem. 40 (2005) 2263–2283.
[2] C. Leonard, J.H. Ferrasse, O. Boutin, S. Lefevre, A. Viand, Bubble column reactors for high pressures and high temperatures operation, Chem. Eng. Res. Des. 100 (2015) 391–421.
[3] A. Youssef Ahmed, H. Al-Dahhan Muthanna, P. Dudukovic Milorad, Bubble columns with internals: a review, Int. J. Chem. Reactor Eng. 11 (2013) 169.
[4] I. Kataoka, M. Ishii, Drift flux model for large diameter pipe and new correlation for pool void fraction, Int. J. Heat Mass Trans. 30 (1987) 1927–1939.
[5] C.S. Brooks, S.S. Paranjape, B. Ozar, T. Hibiki, M. Ishii, Two-group drift-flux model for closure of the modified two-fluid model, Int. J. Heat Fluid Flow 37 (2012) 196–208.
[6] M.E. Shawkat, C.Y. Ching, Liquid turbulence kinetic energy budget of co-current bubbly flow in a large diameter vertical pipe, J. Fluids Eng. 133 (2011) 091303.
[7] G. Besagni, G.R. Guédon, F. Inzoli, Annular gap bubble column: experimental investigation and computational fluid dynamics modeling, J. Fluids Eng. 138 (2016) 011302.
[8] G. Besagni, G. Guédon, F. Inzoli, Experimental investigation of counter current air-water flow in a large diameter vertical pipe with inners, J. Physics: Conf. Ser. 547 (2014) 012024.
[9] A. Sundaresan, Y. Varma, Dispersed phase holdup and bubble size distributions in gas–liquid cocurrent upflow and countercurrent flow in reciprocating plate column, Canad. J. Chem. Eng. 68 (1990) 560–568.
[10] R.T. Rodrigues, J. Rubio, New basis for measuring the size distribution of bubbles, Miner. Eng. 16 (2003) 757–765.
[11] A. Busciglio, F. Grisafi, F. Scargiali, A. Brucato, On the measurement of local gas hold-up and interfacial area in gas–liquid contactors via light sheet and image analysis, Chem. Eng. Sci. 65 (2010) 3699–3708.
[12] C. Xu, T. Shepard, Digital Image Processing Algorithm for Determination and Measurement of In-Focus Spherical Bubbles, in: ASME 2014 4th Joint US-European Fluids Engineering Division Summer Meeting collocated with the ASME 2014 12th International Conference on Nanochannels, Microchannels, and Minichannels, American Society of Mechanical Engineers, 2014, pp. V01BT22A002-V001BT022A002.
[13] S. Guet, S. Luther, G. Ooms, Bubble shape and orientation determination with a four-point optical fibre probe, Exp. Therm. Fluid Sci. 29 (2005) 803–812.
[14] H. Essadki, I. Nikov, H. Delmas, Electrochemical probe for bubble size prediction in a bubble column, Exp. Therm. Fluid Sci. 14 (1997) 243–250.
[15] E. Winkel, S. Ceccio, D. Dowling, M. Perlin, Bubble-size distributions produced by wall injection of air into flowing freshwater, saltwater and surfactant solutions, Exp. Fluids 37 (2004) 802–810.
[16] T. Shepard, E. Ruud, H. Kinane, Wall Shear Effect on Bubble Formation in Turbulent Flows, in: ASME 2013 Fluids Engineering Division Summer Meeting, American Society of Mechanical Engineers, 2013, pp. V01CT17A010-V001CT017A010.
[17] T.G. Shepard, Bubble size effect on effervescent atomization, in: UNIVERSITY OF MINNESOTA, 2011.
[18] A. Karn, C. Ellis, R. Arndt, J. Hong, An integrative image measurement technique for dense bubbly flows with a wide size distribution, Chem. Eng. Sci. 122 (2015) 240–249.
[19] J. Rodríguez-Rodríguez, C. Martínez-Bazán, J.L. Montañes, A novel particle tracking and break-up detection algorithm: application to the turbulent break-up of bubbles, Meas. Sci. Technol. 14 (2003) 1328.
[20] A. Lecuona, P.A. Sosa, P.A. Rodríguez, R.I. Zequeira, Volumetric characterization of dispersed two-phase flows by digital image analysis, Meas. Sci. Technol. 11 (2000) 1152.
[21] Y.M. Lau, K.T. Sujatha, M. Gaeini, N.G. Deen, J.A.M. Kuipers, Experimental study of the bubble size distribution in a pseudo-2D bubble column, Chem. Eng. Sci. 98 (2013) 203–211.
[22] A. Zaruba, E. Krepper, H.M. Prasser, E. Schleicher, Measurement of bubble velocity profiles and turbulent diffusion coefficients of the gaseous phase in rectangular bubble column using image processing, Exp. Therm. Fluid Sci. 29 (2005) 851–860.
[23] Y.M. Lau, N.G. Deen, J.A.M. Kuipers, Development of an image measurement technique for size distribution in dense bubbly flows, Chem. Eng. Sci. 94 (2013) 20–29.
[24] R. Schäfer, C. Merten, G. Eigenberger, Bubble size distributions in a bubble column reactor under industrial conditions, Exp. Therm. Fluid Sci. 26 (2002) 595–604.
[25] A. Shaikh, M.H. Al-Dahhan, A review on flow regime transition in bubble columns, Int. J. Chem. Reactor Eng. 5 (2007).
[26] S. Nedeltchev, A. Shaikh, A new method for identification of the main transition velocities in multiphase reactors based on information entropy theory, Chem. Eng. Sci. 100 (2013) 2–14.
[27] N. Zuber, J.A. Findlay, Average volumetric concentration in two-phase flow systems, J. Heat Trans. 87 (1965) 453–468.
[28] G.B. Wallis, One-dimensional two-phase flow, New York, 1969.
[29] M.R. Bhole, J.B. Joshi, Stability analysis of bubble columns: Predictions for regime transition, Chem. Eng. Sci. 60 (2005) 4493–4507.
[30] G.K. Batchelor, A new theory of the instability of a uniform fluidized-bed, J. Fluid Mech. 193 (1988) 75–110.
[31] A.I. Shnip, R.V. Kolhatkar, D. Swamy, J.B. Joshi, Criteria for the transition from the homogeneous to the heterogeneous regime in 2-dimensional bubble column reactors, Int. J. Multiphase Flow 18 (1992) 705–726.
[32] J.B. Joshi, N.S. Deshpande, M. Dinkar, D.V. Phanikumar, Hydrodynamic stability of multiphase reactors, in: Advances in Chemical Engineering, Academic Press, 2001, pp. 1–130.
[33] M.R. Bhole, S.V. Ghatage, J.B. Joshi, Comments on the paper 'Destabilisation of homogeneous bubbly flow in an annular gap bubble column', in: Fahd M. Al-Oufi, Ian W. Cumming, Chris D. Rielly (Eds.), Can. J. Chem. Eng. 88(4), 482–490 (2010), The Canadian Journal of Chemical Engineering, 89 (2011) 1321–1323.
[34] S.V. Ghatage, M.R. Bhole, N. Padhiyar, J.B. Joshi, G.M. Evans, Prediction of regime transition in three-phase sparged reactors using linear stability analysis, Chem. Eng. J. 235 (2014) 307–330.
[35] M. Carrara, Indagine sperimentale su flussi bifase in colonne verticali, in: Department of Energy, Politecnico di Milano, 2014.
[36] R. Krishna, M.I. Urseanu, A.J. Dreher, Gas hold-up in bubble columns: influence of alcohol addition versus operation at elevated pressures, Chem. Eng. Process.: Process Intensif. 39 (2000) 371–378.
[37] J.F. Richardson, W.N. Zaki, Sedimentation and fluidisation: Part I, Chem. Eng. Res. Des. 75 (Supplement) (1997) S82–S100.
[38] F.M. Aloufi, An investigation of gas void fraction and transition conditions for two-phase flow in an annular gap bubble column, Loughborough University, 2011.
[39] M. Honkanen, P. Saarenrinne, T. Stoor, J. Niinimäki, Recognition of highly overlapping ellipse-like bubble images, Meas. Sci. Technol. 16 (2005) 1760.
[40] P.L.C. Lage, R.O. Espósito, Experimental determination of bubble size distributions in bubble columns: prediction of mean bubble diameter and gas hold up, Powder Technol. 101 (1999) 142–150.
[41] P. Wongsuchoto, T. Charinpanitkul, P. Pavasant, Bubble size distribution and gas–liquid mass transfer in airlift contactors, Chem. Eng. J. 92 (2003) 81–90.
[42] R. Rakoczy, S. Masiuk, Experimental study of bubble size distribution in a liquid column exposed to a rotating magnetic field, Chem. Eng. Process.: Process Intensif. 48 (2009) 1229–1240.
[43] W. Hanselmann, E. Windhab, Flow characteristics and modelling of foam generation in a continuous rotor/stator mixer, J. Food Eng. 38 (1998) 393–405.
[44] A.D. Passos, V.P. Voulgaropoulos, S.V. Paras, A.A. Mouza, The effect of surfactant addition on the performance of a bubble column containing a non-Newtonian liquid, Chem. Eng. Res. Des. 95 (2015) 93–104.
[45] D. Lucas, R. Rzehak, E. Krepper, T. Ziegenhein, Y. Liao, S. Kriebitzsch, P. Apanasevich, A strategy for the qualification of multi-fluid approacheds for nuclear reactor safety, Nucl. Eng. Des. (2015).
[46] T. Ziegenhein, R. Rzehak, D. Lucas, Transient simulation for large scale flow in bubble columns, Chem. Eng. Sci. 122 (2015) 1–13.
[47] M. Pourtousi, P. Ganesan, J.N. Sahu, Effect of bubble diameter size on prediction of flow pattern in Euler–Euler simulation of homogeneous bubble column regime, Measurement 76 (2015) 255–270.
[48] Y. Bian, F. Dong, W. Zhang, H. Wang, C. Tan, Z. Zhang, 3D reconstruction of single rising bubble in water using digital image processing and characteristic matrix, Particuology 11 (2013) 170–183.
[49] D.L. Sahagian, A.A. Proussevitch, 3D particle size distributions from 2D observations: stereology for natural applications, J. Volcanol. Geotherm. Res. 84 (1998) 173–196.
[50] M.I. Urseanu, Scaling up bubble column reactors, 2000.
[51] S. Nedeltchev, M. Schubert, Statistical validation of the mixing length concept in bubble columns operated in the transition flow regime, J. Chem. Eng. Jpn. 48 (2015) 107–111.
[52] T. Otake, S. Tone, K. Shinohara, Gas holdup in the bubble column with cocurrent and countercurrent gas-liquid flow, J. Chem. Eng. Jpn. 14 (1981) 338–340.
[53] K. Yamaguchi, Y. Yamazaki, Characteristics of counter current gas–liquid two-phase flow in vertical tubes, J. Nucl. Sci. Technol. 19 (1982) 985–996.
[54] K. Akita, F. Yoshida, Gas holdup and volumetric mass transfer coefficient in bubble columns, Ind. Eng. Chem. Process Des. Develop. 12 (1973) 76–80.
[55] C.P. Ribeiro Jr, D. Mewes, The influence of electrolytes on gas hold-up and regime transition in bubble columns, Chem. Eng. Sci. 62 (2007) 4501–4509.
[56] F.M. Al-Oufi, C.D. Rielly, I.W. Cumming, An experimental study of gas void fraction in dilute alcohol solutions in annular gap bubble columns using a four-point conductivity probe, Chem. Eng. Sci. 66 (2011) 5739–5748.
[57] F.M. Al-Oufi, I.W. Cumming, C.D. Rielly, Destabilisation of homogeneous bubbly flow in an annular gap bubble column, Canad. J. Chem. Eng. 88 (2010) 482–490.
[58] R.F. Mudde, W.K. Harteveld, H.E.A. van den Akker, Uniform flow in bubble columns, Ind. Eng. Chem. Res. 48 (2009) 148–158.

[59] P. Dargar, A. Macchi, Effect of surface-active agents on the phase holdups of three-phase fluidized beds, Chem. Eng. Process.: Process Intensif. 45 (2006) 764–772.
[60] P. Rollbusch, M. Becker, M. Ludwig, A. Bieberle, M. Grünewald, U. Hampel, R. Franke, Experimental investigation of the influence of column scale, gas density and liquid properties on gas holdup in bubble columns, Int. J. Multiphase Flow 75 (2015) 88–106.
[61] J. Zahradník, M. Fialová, The effect of bubbling regime on gas and liquid phase mixing in bubble column reactors, Chem. Eng. Sci. 51 (1996) 2491–2500.
[62] G. Besagni, F. Inzoli, Influence of electrolyte concentration on holdup, flow regime transition and local flow properties in a large scale bubble column, in: 33rd UIT Heat Transfer Conference, L'Aquila, Italy, 2015.
[63] D. Lucas, E. Krepper, H.M. Prasser, Evolution of flow patterns, gas fraction profiles and bubble size distributions in gas–liquid flows in vertical tubes, Trans. Inst. Fluid-Flow Mach. 112 (2003) 37–46.
[64] J.R. Hernandez-Aguilar, R.G. Coleman, C.O. Gomez, J.A. Finch, A comparison between capillary and imaging techniques for sizing bubbles in flotation systems, Miner. Eng. 17 (2004) 53–61.
[65] R. Parthasarathy, N. Ahmed, Bubble size distribution in a gas sparged vessel agitated by a Rushton turbine, Ind. Eng. Chem. Res. 33 (1994) 703–711.
[66] E. Krepper, D. Lucas, T. Frank, H.-M. Prasser, P.J. Zwart, The inhomogeneous MUSIG model for the simulation of polydispersed flows, Nucl. Eng. Des. 238 (2008) 1690–1702.
[67] Y.M. Lau, W. Bai, N.G. Deen, J.A.M. Kuipers, Numerical study of bubble break-up in bubbly flows using a deterministic Euler–Lagrange framework, Chem. Eng. Sci. 108 (2014) 9–22.
[68] T. Okawa, T. Tanaka, I. Kataoka, M. Mori, Temperature effect on single bubble rise characteristics in stagnant distilled water, Int. J. Heat Mass Trans. 46 (2003) 903–913.
[69] R.M. Wellek, A.K. Agrawal, A.H.P. Skelland, Shape of liquid drops moving in liquid media, AIChE J. 12 (1966) 854–862.
[70] D.W. Moore, The rise of a gas bubble in a viscous liquid, J. Fluid Mech. 6 (1959) 113–130.
[71] T.D. Taylor, A. Acrivos, On the deformation and drag of a falling viscous drop at low Reynolds number, J. Fluid Mech. 18 (1964) 466–476.
[72] T. Tadaki, S. Maeda, On the shape and velocity of single air bubbles rising in various liquids, Kagaku Kogaku 25 (1961) 254–264.
[73] R. Clift, J.R. Grace, M.E. Weber, Bubbles, drops, and particles, New York, 1978.
[74] G. Bozzano, M. Dente, Shape and terminal velocity of single bubble motion: a novel approach, Comput. Chem. Eng. 25 (2001) 571–576.
[75] N.H. Hoang, D.J. Euh, B.J. Yun, C.H. Song, A new method of relating a chord length distribution to a bubble size distribution for vertical bubbly flows, Int. J. Multiphase Flow 71 (2015) 23–31.
[76] G.P. Celata, M. Cumo, F. D'Annibale, P. Di Marco, A. Tomiyama, C. Zovini, Effect of gas injection mode and purity of liquid on bubble rising in two-component systems, Exp. Therm. Fluid Sci. 31 (2006) 37–53.
[77] G.P. Celata, M. Cumo, F. D'Annibale, A. Tomiyama, The wake effect on bubble rising velocity in one-component systems, Int. J. Multiphase Flow 30 (2004) 939–961.
[78] G.P. Celata, F. D'Annibale, P. Di Marco, G. Memoli, A. Tomiyama, Measurements of rising velocity of a small bubble in a stagnant fluid in one- and two-component systems, Exp. Therm. Fluid Sci. 31 (2007) 609–623.
[79] L.S. Fan, K. Tsuchiya, Bubble Wake Dynamics in Liquids and Liquid–Solid Suspensions, Butterworth-Heinemann, Oxford, 1990.
[80] J.C. Cano-Lozano, P. Bohorquez, C. Martínez-Bazán, Wake instability of a fixed axisymmetric bubble of realistic shape, Int. J. Multiphase Flow 51 (2013) 11–21.
[81] J.B. Joshi, Solid–liquid fluidised beds: some design aspectS, Chem. Eng. Res. Des. 61 (1983) 143–161.
[82] A.V. Nguyen, Prediction of bubble terminal velocities in contaminated water, AIChE J. 44 (1998) 226–230.
[83] J. Magnaudet, I. Eames, The motion of high-Reynolds-mumber bubbles in inhomogeneous flows, Annu. Rev. Fluid Mech. 32 (2000) 659–708.
[84] N. Zuber, On the dispersed two-phase flow in the laminar flow regime, Chem. Eng. Sci. 19 (1964) 897–917.
[85] I. Reilly, D. Scott, T. Debruijn, D. MacIntyre, The role of gas phase momentum in determining gas holdup and hydrodynamic flow regimes in bubble column operations, Canad. J. Chem. Eng. 72 (1994) 3–12.
[86] P.M. Wilkinson, A.P. Spek, L.L. van Dierendonck, Design parameters estimation for scale-up of high-pressure bubble columns, AIChE J. 38 (1992) 544–554.
[87] H.M. Letzel, J.C. Schouten, R. Krishna, C.M. van den Bleek, Gas holdup and mass transfer in bubble column reactors operated at elevated pressure, Chem. Eng. Sci. 54 (1999) 2237–2246.
[88] J.F. Walter, H.W. Blanch, Bubble break-up in gas—liquid bioreactors: break-up in turbulent flows, Chem. Eng. J. 32 (1986) B7–B17.
[89] R.P. Hesketh, T.W. Fraser Russell, A.W. Etchells, Bubble size in horizontal pipelines, AIChE J. 33 (1987) 663–667.